A CRYSTALLOGRAPHIC STUDY OF SOME PYROPHOSPHATES

AN X-RAY CRYSTALLOGRAPHIC STUDY OF $Na_4P_2O_7$ $Ba_2P_2O_7$ AND $H_4P_2O_7$

AN X RAY CRYSTALLOGRAPHIC STUDY OF $Na_4P_2O_7$, $Ba_2P_2O_7$ AND $H_4P_2O_7$

by

DOUGLAS JOHN DE LA MATTER, B.Sc.

A Thesis

Submitted to the Faculty of Graduate Studies

in Partial Fulfilment of the Requirements

for the Degree

Master of Science

McMaster University

January, 1972

MASTER OF SCIENCE (1972) McMASTER UNIVERSITY,
(Chemistry) Hamilton, Ontario.

TITLE: An X-Ray Crystallographic Study of $Na_4P_2O_7$, δ-$Ba_2P_2O_7$ and $H_4P_2O_7$

AUTHOR: Douglas John De La Matter, B.Sc. (McMaster University)

SUPERVISOR: Professor C. Calvo

NUMBER OF PAGES: vii, 116

SCOPE AND CONTENTS:

The symmetries and unit cell dimensions of crystals of $Na_4P_2O_7$, δ-$Ba_2P_2O_7$ and $H_4P_2O_7$ have been determined by X-ray diffraction methods. Changes in symmetry and unit cell dimensions of $Na_4P_2O_7$ as a function of temperature have been described and a model has been proposed describing the statistics of these changes. The existence of disorder in the crystal structure of δ-$Ba_2P_2O_7$ has been established and the unit cell dimensions of a previously unreported low temperature form are reported.

ACKNOWLEDGEMENTS

I wish to express my gratitude to my supervisor Professor C. Calvo for constantly providing his valuable and friendly assistance throughout this research. I am also grateful to the other members of the crystallography group, especially Mr. R. Gopal and Mr. K. Y. Leung for their cooperation and the many helpful discussions we had together. Mrs. H. Kennelly was the cheerful and efficient typist.

Finally, many thanks go to my wife for her patience and optimism during the work on this thesis.

TABLE OF CONTENTS

INDEX OF TABLES

INDEX OF ILLUSTRATIONS

CHAPTER I

GENERAL INTRODUCTION

In this research, investigations into the crystal structures of three types of pyrophosphate compounds have been initiated. Such structures, including the pyrophosphates anion are of interest for several reasons.

Crystallographically the $P_2O_7^{4-}$ ion represents a class of structures similar to compounds containing discrete PO_4^{3-} tetrahedra but with an added restriction on their relative positions and orientations due to the fact that every pair of PO_4^{3-} groups must share a common oxygen. This indicates that a smaller number of basic structural types may occur.

Extensive work has already been done in relating structural types to the relative sizes of cations in compounds of the type $M_2X_2O_7$. Felsche (1) has examined a series of rare-earth disilicates ($M_2Si_2O_7$) in which the cations vary in ionic radius from 1.06 Å to 0.85 Å due to the lanthanide contraction, yet show uniform chemical properties. Seven different structural types were observed within the series. Recently, Baglio and Dann (2) have correlated a large number of $M_2X_2O_7$ structures into three major structural groups, according to size of both the cation M and the X part of the

anion. Those compounds in which the ionic radius of X is greater than $\sim$ 0.5 Å crystallize with structures related to that of atopite, where the coordination number of X is 6. If the ionic radius of X is less than 0.5 Å, its coordination number will be 4 and the size of the cation M determines whether the structure will be related to thortveitite or the dichromate-type structures. If the ionic radius of M is less than $\sim$ 0.8 Å a pyrophosphate compound should crystallize in the thortveitite structure with the anion lying in a staggered conformation relative to the terminal oxygen atoms. When M is greater than $\sim$ 0.8 Å, the structure should be of the dichromate type and the terminal oxygen atoms of the anion will be eclipsed. $Ba_2P_2O_7$ is expected to show similarities to the dichromate series of structures. The trend of the rare earth silicates to adopt structures of higher symmetry with increasing cationic radius is reversed in the cases of α-$Ca_2P_2O_7$ and α-$Sr_2P_2O_7$. $Ba_2P_2O_7$ may continue this anomalous trend.

Anhydrous sodium pyrophosphate crystals are also interesting from the standpoint of cation size. Sodium is intermediate in size relative to the cation size determining each of the two classes of structures found in the pyrophosphate series. When the cation is of an intermediate size, phase transformations are likely to occur as a function of temperature since it is too large to fit easily into inter-

stitial sites and too small to act as an element of the structure and pack in a similar fashion to the oxygen atoms. $Na_4P_2O_7$ should be an excellent illustration of this situation since four distinct phase transformations have been reported for the compound as a function of temperature (3). The mechanics and energetics of such transitions can only be fully understood when the details of the crystal structures within each phase are known.

Cruickshank (4) has discussed the nature of $p\pi$-$d\pi$ bonding and its relation to the bridging bond angle in the anion $X_2O_7^{n-}$ where x represents chlorine, sulphur, silicon or phosphorous. He has related this discussion to conformations of Cl_2O_7 found in the gas phase and of $S_2O_7^{2-}$ found in crystalline $K_2S_2O_7$, as well as the conformation of $P_2O_7^{4-}$ in the crystalline $Na_4P_2O_7 \cdot 10H_2O$. His discussion used valence bond approximations for the anion and thus ignored the influence of the environment. A test of these approximations could be provided by a detailed knowledge of the structure of $Na_4P_2O_7$ in the anhydrous crystal. A comparison of the structures of the decahydrate and the anhydrous compound may reveal the extent of any role played by the water molecules in influencing the shape of the anion.

Cruickshank's discussion makes no attempt to predict the effect of the cation distribution in the crystal on the

bond lengths and angles in the anion. Baur (5) on the other hand, has correlated characteristics of structures of the type $M_nX_rO_s$ from just such a viewpoint. He makes the assumption that only electrostatic interactions are significant between cation and anion. For the cases in which M = Zn, Cu, Mg, Mn this assumption may or may not be justified depending on the extent to which the d-orbitals of the cation interact with the anion. For the case of M = Na however, the assumption is almost certainly justified and so, correlations between Baur's predicted bond lengths and angles in the anion and those exhibited by crystalline $Na_4P_2O_7$ would be a valuable test of the accuracy of those predictions.

It would be of interest as well, to compare the effects of Na^+ and H^+ on the details of the P-O bonds in P_2O_7. The covalent nature of the P-O-(H) bond is fairly easily characterized and the cation-oxygen distance is not restricted by packing considerations and size effects. Further, it would be valuable, both in Cruickshank's discussion and in numerous other studies, to know the "equilibrium" configuration of the pyrophosphate anion, that is, the configuration that would be assumed if no influence were exerted by cations. Beagley (6) has reported the configuration for Cl_2O_7 in the gas phase, and a theoretical study by D. B. Boyd (7) of the electron density distribution in $P_2O_7^{4-}$ has been completed.

Neither investigation gives a reliable indication of the $P_2O_7^{4-}$ "equilibrium" configuration in the crystal environment however. Thus a determination of the crystal structure of $H_4P_2O_7$ was attempted. Such a determination would not only act as experimental correlation for the theoretical study, but also show the anion conformation when effects of cation size have been minimized.

CHAPTER II

CRYSTAL STRUCTURE ANALYSIS

A single crystal can be considered as a large number of parallelopipeds whose atomic arrangements are identical over time periods small in comparison with the duration of the observation. The smallest parallelopiped that satisfies the required translational periodicity is called the unit cell and its edges can be described by a set of three non-coplanar vectors $\underline{a}$, $\underline{b}$ and $\underline{c}$.

The position of any point in the crystal lattice can be specified by a vector from a given origin to that point in the lattice such that

$$\underline{r} = \underline{p} + n_1\underline{a} + n_2\underline{b} + n_3\underline{c} \qquad [2.1]$$

where n_1, n_2 and n_3 are integers and $\underline{p}$ is a vector within the unit cell whose origin is at the chosen origin of the cell. The path difference between two waves of plane parallel radiation, scattered from two different points in the crystal lattice will be

$$\lambda\underline{r} \cdot \underline{H} \qquad [2.2]$$

where λ is the wave length of the radiation and $\underline{H}$ is the difference between the direction vectors for the incident and scattered radiation. In order that the waves be scattered in

phase, the path difference should equal a whole number of waves. Thus, coherent scattering requires that

$$(n_1\underline{a} + n_2\underline{b} + n_3\underline{c})\cdot\underline{H} = \text{integer}$$

Laue's equations follow from this condition:

$$\begin{aligned} \underline{a} \cdot \underline{H} &= h \\ \underline{b} \cdot \underline{H} &= k \\ \underline{c} \cdot \underline{H} &= \ell \end{aligned} \qquad [2.3]$$

where h, k and ℓ are integers. When all three of Laue's equations are satisfied simultaneously, a maximum in the diffraction pattern will occur.

Since the incident radiation is in the form of plane waves, the normal to a set of plane waves constitutes a natural vector system to describe scattering phenomena. Such a system has been defined and is called the reciprocal lattice. Three non-coplanar vectors make up the basis set:

$$\begin{aligned} \underline{a}^* &= \frac{\underline{b} \times \underline{c}}{v} \\ \underline{b}^* &= \frac{\underline{c} \times \underline{a}}{v} \\ \underline{c}^* &= \frac{\underline{a} \times \underline{b}}{v} \end{aligned} \qquad [2.4]$$

where $v = \underline{a} \cdot (\underline{b} \times \underline{c})$ and represents the volume of the unit cell. The normalization by the cell volume v is convenient, yielding unitless exponential functions when the amplitude of scattering is considered. The scattering vector $\underline{H}$ may now be expressed in terms of this basis set.

$$\underline{H} = h\underline{a}^* + k\underline{b}^* + \ell\underline{c}^* \qquad [2.5]$$

It can be shown that the scattering from a system showing periodicity in all three dimensions requires that h, k and ℓ be integers. Since $\underline{H}$ has previously been defined as the directed difference between incident and scattered radiation, it can be seen that each point in the reciprocal lattice is related to the direction of a diffracted beam of X-rays relative to the incident beam.

X-rays are scattered by the bound electrons of the atoms. Classically, the electric field components of the X-rays cause the electrons to oscillate. The oscillating electrons reemit electromagnetic radiation of the same wavelength. Since the wavelength is comparable to the size of the atoms from which it is scattered, there will be interference effects from radiation scattered by different electrons in the same atom. Thus the ratio of scattering in the direction $\underline{H}$ of an atom at the origin to that of an electron at the origin is given by:

$$\frac{\underline{E}^{\text{Atom}}}{\underline{E}^{\text{Electron}}} = \int \rho(\underline{r}) \exp(2\pi i \underline{H}\cdot\underline{r}) d\underline{r} \qquad [2.6]$$

This ratio is the atomic scattering factor f_j^o and is evaluated theoretically for an atom at rest, ie. at absolute zero. The electron density function $\rho(\underline{r})$ is calculated theoretically, assuming atoms to be spherically symmetrical.

For an atom at a position $\underline{r}_j$ from the origin, the scattering contribution relative to an electron at the origin is

$$\frac{\underline{E}^{Atom}(\underline{r}_j)}{E^{Electron}} = \int \rho(\underline{r}) \exp(2\pi i \underline{H}\cdot(\underline{r}+\underline{r}_j))d\underline{r}$$

$$= f_j^o \exp(2\pi i \underline{H}\cdot\underline{r}_j) \qquad [2.7]$$

If a sum is taken over all N atoms in one unit cell, the structure factor $F(\underline{H})$ for the cell is obtained.

$$F(\underline{H}) = \sum_{j=1}^{N} f_j^o \exp(2\pi i \underline{H}\cdot\underline{r}_j) \qquad [2.8]$$

It is assumed that each electron is uniquely assignable to an atom.

A more exact expression can be obtained by replacing the assumption of no thermal vibration with a term in the scattering factors of the individual atoms, accounting for the average displacement from the mean position due to thermal motions of the atoms. Since the atomic scattering factor is the Fourier transform of the atomic electron density, any apparent spreading out of the density in real space will lead to a contraction in its Fourier transform. Thus,

$$f_j = f_j^o \exp(-B\cdot\sin^2\theta/\lambda^2) \qquad [2.9]$$

where B is a positive definite quantity called the isotropic temperature factor and is related to the mean square amplitude

of vibration ($\overline{u^2}$)

$$B = 8\pi^2 \overline{u^2} \qquad [2.10]$$

The assumption of isotropic thermal vibration can be removed by introducing anisotropic temperature factors $\underline{\underline{\beta}}_j$ such that

$$f_j = f_j^o \exp(-\underline{H}\cdot\underline{\underline{\beta}}_j\cdot\underline{H}) \qquad [2.11]$$

When referred to the axes of the reciprocal lattice, the exponential term expands to:

$$\exp(b_{11}h^2 + b_{22}k^2 + b_{33}\ell^2 + 2b_{12}hk + 2b_{23}k\ell + 2b_{13}h\ell)$$

where the constants b_{mn} are evaluated for each atom during refinement of the structure.

The total amplitude of scattering from a small single crystal (in which all unit cells are bathed equally in radiation) is given by the sum of the scattering amplitudes over all unit cells, taking into account the phase difference due to the positions of all the atoms in each unit cell

$$F(\underline{H}) = \sum_{n_1}\sum_{n_2}\sum_{n_3=-\infty}^{\infty} \sum_{j=1}^{N} f_j \exp(2\pi i\ \underline{H}\cdot(\underline{r}_j+n_1\underline{a}+n_2\underline{b}+n_3\underline{c})) \qquad [2.12]$$

When translational symmetry rigorously applies, the sum can be separated to give

$$F(\underline{H}) = \sum_{j=1}^{N} f_j \exp 2\pi i\ \underline{H}\cdot\underline{r}_j \sum_{n_1}\sum_{n_2}\sum_{n_3=-\infty}^{+\infty} \exp(2\pi i\ \underline{H}\cdot(n_1\underline{a}+n_2\underline{b}+n_3\underline{c})) \qquad [2.13]$$

where the first sum determines the scattering amplitude from a unit cell and the second summation set determines the relative contributions from unit cells in different parts of the crystal.

Because the unit cells are identical, Laue's equations apply and the equation reduces to:

$$F(\underline{H}) = \sum_{j=1}^{N} f_j \exp(2\pi i(\underline{H}\cdot r_j)) \quad . \qquad [2.14]$$

The scattering from all unit cells is coherent and the phase is determined solely by the positions of the scattering atoms within a unit cell.

The electron density function for the unit cell can be expressed as the Fourier transform of the structure factor which is in the most general case a complex quantity.

$$\rho(x,y,z) = \frac{1}{V} \sum_h \sum_k \sum_{\ell=-\infty}^{+\infty} F(hk\ell)\exp(-2\pi i(hx+ky+\ell z)). \qquad [2.15]$$

Thus, once a complete set of structure factors, including both amplitude and phase information is obtained, the determination of the crystal structure is straightforward.

Unfortunately, the only practical method of observing the structure amplitude is measurement of the intensity (I) of the X-ray beam scattered in a direction given by $\underline{H}$

$$I(\underline{H}) = C(L\cdot p)A\ |F(\underline{H})|^2 \quad . \qquad [2.16]$$

C is a constant dependant on the intensity and wavelength of the incident radiation, and on the volume of the unit cell. Since the crystals used in experiments are actually mosaic, there is a finite range of angle over which one can achieve diffraction maxima. L is the Lorentz factor and normalizes

the speeds at which various reciprocal lattice vectors pass through the reflection condition. p is a term to correct for the partial polarization of the X ray beam resulting from the variation in reflecting efficiency of waves with electric vectors oriented parallel or perpendicular to the plane of reflection. The term A accounts for the attenuation of both the incident and diffracted beam as they pass through the crystal mass, and depends on the absorbing properties of the constituent elements in the crystal. Thus,

$$I(\underline{H}) \propto |F(\underline{H})|^2$$

or more accurately,

$$I(\underline{H}) \propto F(\underline{H})F^*(\underline{H})$$

where $F^*(\underline{H})$ is the complex conjugate of the structure factor.

No direct information about the phase of a reflection is transmitted by a measurement of its intensity. However, since unique geometries for the scattering matter can be derived, information concerning the phases does reside in the relative values of the various scattering amplitudes. It is fruitful, then, to examine these amplitudes to obtain any direct information about the structure that they may contain.

The Patterson Function

If $|F(\underline{H})F^*(\underline{H})|$ is substituted for the phased structure factor in equation 2.15, it can be shown that the resulting expression,

$$P(u,v,w) = \iiint \rho(u,v,w) \cdot \rho(u+x,v+y,w+z)\,dxdydz$$

$$= \frac{1}{v} \sum_h \sum_k \sum_{\ell=\infty}^{+\infty} |F(hk\ell)F^*(hk\ell)| \exp\{2\pi i\,(hu+kv+\ell w)\} \quad [2.17]$$

represents a function whose maxima correspond to vector separations between atoms in the unit cell. (8)

Since $P(u,v,w) = p(-u,-v,-w)$,

$$P(u,v,w) = \frac{1}{v} \sum_h \sum_k \sum_{\ell}^{+\infty}{}_{\infty} |F(hk\ell)F^*(hk\ell)| \cos 2\pi(hu+kv+lw). \quad [2.18]$$

$|F(hk\ell)F^*(hk\ell)|$ has been shown to be proportional to the intensity $I(hk\ell)$ at each reciprocal lattice point and $\langle F(hk\ell)F^*(hk\ell)\rangle$ over all values of $\sin\theta/\lambda$ is dependent on the number of electrons responsible for the scattering. Thus, vectors between heavy atoms (ie. those with many electrons) will give larger maxima than vectors between light atoms.

The Patterson function contains the vector sets $\underline{r}_i - \underline{r}_j$ and one wishes to find a unique set of $\underline{r}_i$. This will be easiest when the structure contains a small number of electron-rich atoms. Light atoms may be resolved by their interaction with any heavy atom in the structure, but they present many more difficulties in the identification of superimposed peaks. Since the summations over h, k and ℓ should extend from $-\infty$ to $+\infty$, Patterson functions produced with limited numbers of data may be subject to series termination errors and thus present further difficulties in resolution of small peaks.

Least Squares Refinement

Approximate atomic positions derived from an analysis of the Patterson function can be considered as a preliminary model of the structure. The phased structure factors expected from this model can be calculated and compared with the observed structure factors. Differences between F_{OBS} and F_{CALC} are minimized by slight adjustments of the atomic positions according to the method of least squares. (9)

The process attempts to minimize a "residual" R with respect to various atomic parameters X_1, X_2 ... X_m such that m simultaneous equations of the form

$$\frac{\partial R}{\partial X_k} = 0$$

are solved.

$$R^2 = \frac{\sum_{i=1}^{N} (|F_{OBS}|^2 - |F_{CALC}|^2)_i \cdot w_i}{\sum_{i=1}^{N} |F_{OBS}|_i^2 \cdot w_i} \qquad [2.19]$$

where $|F_{OBS}|$ and $|F_{CALC}|$ are the observed and calculated values for $|F(\underline{H})|$ and the summation is carried out over N reflections. Each reflection is given a weight w_i which strictly should be

$$w_i = 1/\sigma_i^2 \qquad [2.20]$$

where σ_i is the standard deviation of $|F_{OBS}|_i$.

Difficulties in assigning true σ values to individual

reflections are usually overcome by the use of unit weights, or assuming that $\sigma(F_{OBS})$ depends only on $|F_{OBS}|$. A more realistic scheme proposed by Cruickshank et.al.(10) describes the average weighted discrepancy as a function of $|F_{OBS}|$ or some other systematic parameter.

$$\langle w_i \Delta_i^2 \rangle = \langle w_i ||F_{OBS}| - |F_{CALC}||_i^2 \rangle \qquad [2.21]$$

where the weight is determined by:

$$(w_i)^{-1} = a_o + |F_{OBS}|_i + a_1 |F_{OBS}|_i^2.$$

a_o and a_1 are constants satisfying the functional criterion for $|F_{OBS}|$ and are of the order of $2|F_{MIN}|$ and $\frac{2}{|F_{MAX}|}$ respectively.

Disordered Structures

It is usually possible to treat each unit cell of a crystal as a unique scattering volume, and all unit cells as identical. In this way it is possible to take account of the first three summations in equation 2.12 and set the components of $\underline{H}$ to integers. If imperfections arise in the three dimensional translational periodicity, it is necessary to include the different contributions of each unit cell to the structure amplitude.

Because the frequency of the x-radiation is much higher than the frequency of thermal vibrations, the plane waves "see" an instantaneous picture of the atoms displaced from their

mean positions by various fractions of their amplitudes of vibration. The fraction that any given atom is displaced may vary from one unit cell to the next and thus small deviations from perfect translational periodicity will be observed. However, on the time scale of the normal diffraction experiment, the vibration is very fast and each atom in each unit cell will appear to have the greatest density at the mean position and be elongated in the direction of vibration. The net result is at most a slight decrease in the volume of reciprocal space in which the reflection condition is met. This effect is usually accounted for by the inclusion of a "temperature-factor" term in the expression for the scattering factor of individual atoms. (equation 2.9).

If the displacement from the equilibrium position is relatively constant on the experimental time scale, the observed part of the scattering amplitude will reflect the translational disparity and coherent scattering will no longer be exclusively observed. The expression for the structure amplitude in the direction of scattering $\underline{H}$ is

$$F(\underline{H}) = \sum_{n_1} \sum_{n_2} \sum_{n_3=0}^{+\infty} \sum_{j=1}^{N} f_j \exp 2\pi i \, \underline{H} \cdot [\underline{r}_j(n_1,n_2,n_3) + n_1\underline{a} + n_2\underline{b} + n_3\underline{c}] \qquad [2.12]$$

If the displacements are small and can occur in any direction, the equation may be separated into two parts.

$$F(\underline{H}) = \sum_{n_1}\sum_{n_2}\sum_{n_3=0}^{+\infty}\left\{\sum_{j=1}^{N'} f_j \exp 2\pi i\underline{H}\cdot[\underline{r}_j(n_1,n_2,n_3)+n_1\underline{a}+n_2\underline{b}+n_3\underline{c}]\right.$$

$$\left. + \sum_{j=1}^{N''} f_j \exp 2\pi i\, H\cdot[\underline{r}_j(n_1n_2n_3)+n_1\underline{a}+n_2\underline{b}+n_3\underline{c}]\right\}.$$

The first summation is over all atoms in the crystal residing in "normal" positions (N') that is, positions satisfying translational symmetry exactly, and the second sum is over "displaced" atoms (N") only.

$$I(\underline{H}) = F(\underline{H})F^*(\underline{H})$$

$$= \sum_{j=1}^{N'}\sum_{k=1}^{N'} f_j\, f_k \exp 2\pi i\, \underline{H}\cdot(\underline{r}_j-\underline{r}_k)$$

$$+ \sum_{n_1}\sum_{n_2}\sum_{n_3}\sum_{n_1^*}\sum_{n_2^*}\sum_{n_3^*}\sum_{j=1}^{N'}\sum_{k=1}^{N''} f_j\, f_k \exp 2\pi i\, \underline{H}\cdot(\underline{r}_j-\underline{r}_k)$$

$$\exp 2\pi i\, \underline{H}\cdot[(n_1-n_1^*)\underline{a} + \ldots.]$$

$$+ \sum_{n_1}\sum_{n_2}\sum_{n_3}\sum_{n_1^*}\sum_{n_2^*}\sum_{n_3^*}\sum_{j=1}^{N''}\sum_{k=1}^{N''} f_j\, f_k \exp 2\pi i\, \underline{H}(r_j-r_k)$$

$$\exp 2\pi i\, \underline{H}\cdot[(n_1-n_1^*)\underline{a} + \ldots] \,. \qquad [2.22]$$

The first term contributes to the intensity only at the Bragg peak (where the components of $\underline{H}$ are integers). The second term involves vector differences between displaced atoms and undisplaced ones. If the displacements are random throughout the crystal, the vector sum of the displacements

will have an average contribution of zero. The third sum can be rearranged to add all contributions from cells separated by a given vector and the contribution will be:

$$f_j f_k [(P_{AA}+P_{BB}+....) \exp 2\pi i \underline{H}\cdot 0 + P_{AB} \exp 2\pi i \underline{H}\cdot(\underline{r}_A-\underline{r}_B)$$

$$+ P_{BA} \exp 2\pi i \underline{H}\cdot(\underline{r}_B-\underline{r}_A) + P_{AC} \exp 2\pi i \underline{H}\cdot(\underline{r}_A-\underline{r}_C)$$

$$+ \text{etc.}]$$

where P_{xy} is the probability of a displacement x occurring in the first cell and y in the next cell.

Thus the contribution to the intensity of the scattered radiation is not limited only to positions in reciprocal space satisfied by Laue's equations, but may result in intensity occurring as diffuse streaks in positions between the discrete reciprocal lattice points.

The most common example of disorder is that caused by stacking faults in the crystal. The intensity distribution resulting from this kind of defect is observed as diffuse streaks lying parallel to the direction in which the faults occur.

CHAPTER III

METHODS OF DATA COLLECTION AND RELATED APPARATUS

Two methods of data collection were used to investigate the compounds in question - photographic film techniques and scintillation counting techniques.

Photographic Methods:

Intensity data collected by this method was obtained from films exposed on a Buerger Precession Camera equipped with an integrating mechanism (manufactured by Charles A. Supper Co.). The film, held in a planar cassette, may be set at various distances up to 60 mm. from the crystal. The largest distance is used for zero layer photographs and the film is moved towards the crystal to record upper layer photographs. The camera linkages are arranged so that the film always remains parallel to the reciprocal lattice plane being photographed, as the crystal is oscillated in the X-ray beam.

To isolate only reflections from one reciprocal lattice plane, a flat metal plate with a ring cut in it is placed parallel to the film and between it and the crystal. The relationship between μ, the angle through which the crystal is oscillated; r_s the radius of the layer-screen ring; s, the

screen to crystal distance setting; and d, the distance by which the film is advanced towards the crystal (the upper level height) is

$$s = r_s \cot \cos^{-1} (\cos \mu - d).$$

For a zero level photograph d = 0 and the formula reduces to

$$s = r_s \cot \mu.$$

Tables of setting data are compiled in Volume II of the International Tables of Crystallography (9), to facilitate use of the camera.

The integrating mechanism on the camera enables the intensities of reflections to be measured by an optical densitometer. This mechanism displaces the film cassette by a series of 144 small increments so that the diffracted beam traces over a square pattern on the film - 12 increments per side, and produces a regular and conveniently shaped spot at each reflection site. The relative optical densities of the spots are then measured with a microdensitometer.

The microdensitometer used for collecting film data was of the double-beam type (manufactured by Joyce Loebl and Co. Ltd.). One beam of light is passed through the sample to be measured while the other passes through a continuous density wedge. The intensities of the two beams are compared by photoelectric detectors and any resulting imbalance activates a mechanical drive that adjusts the wedge until the intensities

are equal. A recorder pen is linked to the position of the wedge and thus a graphical plot of optical density vs. position on the film can be made simply by advancing the film through the measuring beam and graph paper under the pen simultaneously. The heights of peaks produced in this manner give relative intensities of all the reflections on a film.

In order that both the strongest and the weakest reflections in a given layer are measurable, a range of exposures of each layer line is taken, usually 1, 3 and 9 cycles of the integrating mechanism (144 minutes per cycle).

The relative intensities measured in this way are corrected for Lorentz and polarization factors and converted to structure factors for use in least-squares refinement of the crystal structure.

Counting Methods:

One projection of the $Na_4P_2O_7$ data and all of the final data for $Ba_2P_2O_7$ were collected by scintillation counter techniques. The former were collected on a manual single crystal diffractometer constructed from a Weissenberg camera (manufactured by Charles A. Supper Co.) on which a scintillation counter was mounted with freedom to follow an arc in 2θ centred on the spindle axis of the camera. Standard equi-inclination Weissenberg geometry (11) was employed and reflections were measured by the "ω" scan technique (12) in which

the counter position is fixed in a given 2θ and ϕ and the crystal is then rocked in a manner that the reciprocal lattice point in question crosses the surface of the Ewald sphere twice during each observation. Approximate angular coordinates 2θ and ϕ were measured for each reflection from a Weissenberg photograph. Exposures of 48 hours revealed all reflections that were observable above background with the scintillation counter.

Each X-ray photon passing into the counter produced a pulse whose amplitude was proportional to the energy of the incident photon. After suitable amplification the pulse passed through a discriminator circuit. This circuit had an electronic window, accepting pulses only between preset upper and lower voltage limits and thus eliminating low energy background noise and any extranneous high amplitude noise produced by neighboring electrical equipment. The counter had been calibrated for "dead-time" effects and was found to give a linear response when counting at 3 times the rate of the strongest reflection measured in this data set (13). No dead time corrections were applied to the data. A more complete description of the operation of the instrument may be found elsewhere (14).

All final data from the room temperature structure of $Ba_2P_2O_7$ were collected on a General Electric Semi Automatic XRD6 single crystal X-ray diffractometer. This apparatus was equipped with an Eulerian cradle type of crystal support and

Figure 3.1

Illustration of the geometry employed by Eulerian cradle type of crystal support

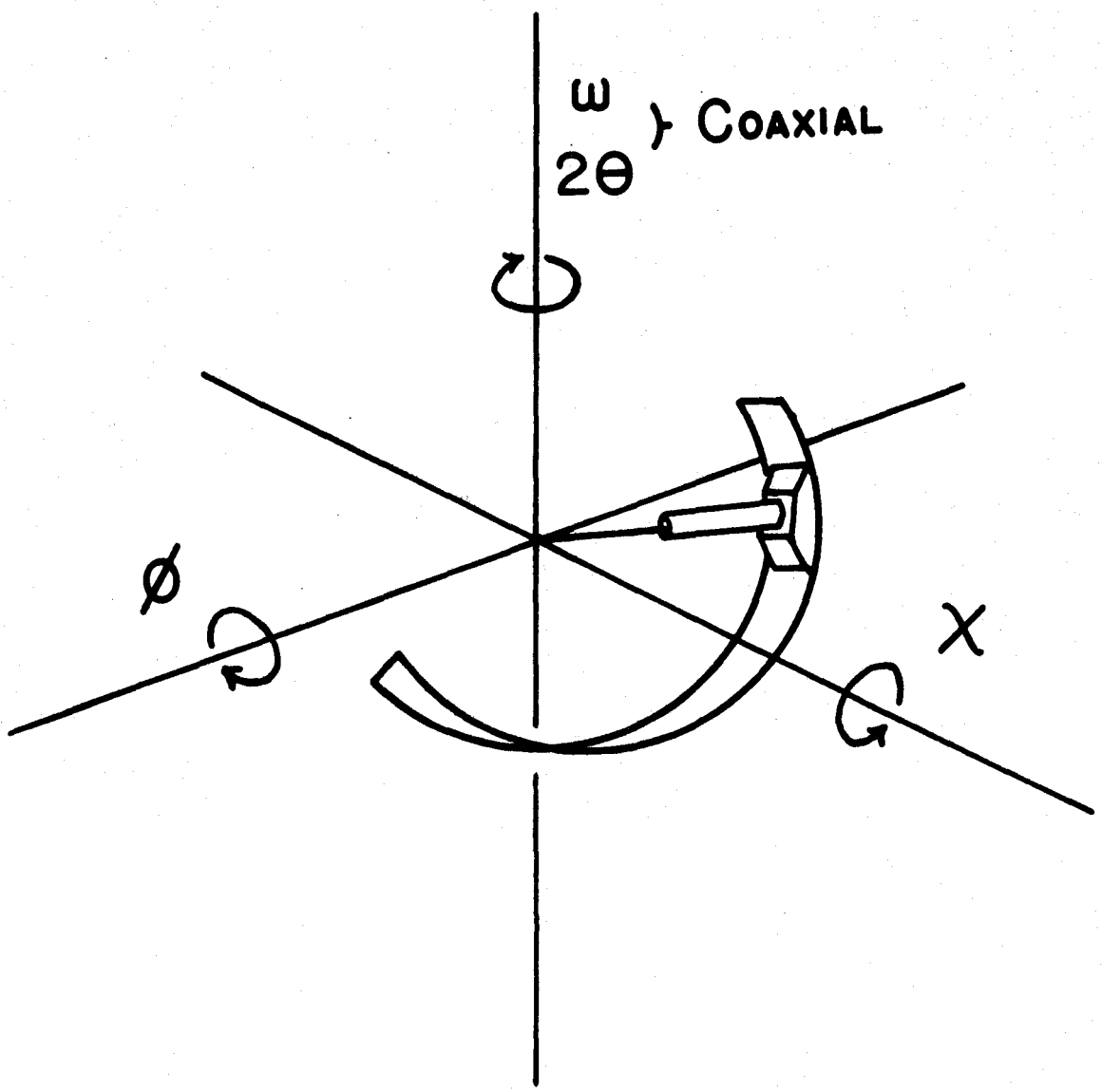
ω
2θ
COAXIAL
ø
χ

required a eucentric goniometer head. An illustration of the geometry appears in Fig. 3.1 . Since the scintillation counter is restricted to rotation about a single vertical axis, the incident and diffracted rays being measured must lie in a horizontal plane. To position any reflection within the counter aperture, the Eulerian angles ϕ, χ and ω must be adjusted so that the reciprocal lattice point of interest is in the plane of the counter. This allows zero-level Weissenberg geometry to be applied. For any fixed ω there are unique settings of 2θ, ϕ and χ to position each reflection on the counter.

About 30 reflections were centered manually and the setting angles were recorded. These angles were then refined by the least squares program GELSA (15) and angular settings for each reflection to be observed were calculated and recorded on punched cards using the program DIFPCH (15)

Intensities were recorded with Zr-filtered MoKα radiation using a 2θ scan at a rate of two degrees per minute. Background counts were taken at each extremity of the scan for 20 seconds duration. The scan width was determined from the equation

$$\text{scan} = A + B \tan\theta \qquad [3.1]$$

with constants A and B assigned values of 1.80 and 1.00 respectively. Factors influenced by the physical characteristics of the crystal such as size, mosaicity, etc. are considered

in the value assigned to A, while the value of B indicates factors, such as dispersion, that are a function of theta (12)

Seven standard reflections that were well distributed in reciprocal space, were used to check periodically for change in crystal alignment or possible crystal deterioration. The intensities of these standard reflections did not show any significant variation during the course of the measurements. The data were recorded in six concentric shells up to a maximum scattering angle (2θ) of 60°. Considering the hexagonal symmetry of the crystal, only one hemisphere in reciprocal space was examined out to a scattering angle of $2\theta = 35°$. Beyond this point only a quarter-hemisphere was observed. In this way a total of 2287 reflections were measured, 332 of these belonging to a unique set.

The measured intensities were corrected for Lorentz and polarization factors in the form corresponding to the equatorial geometry of the measurements:

$$L_p = (1 + \cos^2 2\theta)/2 \sin \theta. \qquad [3.2]$$

The resulting quantities were reduced to their square roots, yielding the absolute values of the structure factors associated with each observed lattice point in reciprocal space. These steps in data reduction were completed using the computer program DATRDN (15).

The information was then transferred to punched cards

and used in the standard least-squares and Fourier computer programs of the laboratory.

High Temperature Apparatus:

Investigations at high temperatures were carried out using a simple arrangement of coiled nichrome wire mounted on the collimator of a precession camera. One set of parallel turns of heating wire was suspended about 0.75 cm. below the crystal and another 0.75 cm .above. Each coil extended laterally for about 2 cm. on either side of centre and was 1.5 cm wide. Thus there was ample room to position the crystal in a thermally equilibrated site within the heating envelope. The coils did place some limitation on the freedom to adjust the goniometer arcs. A chromel-alumel thermocouple was installed as close as possible to the crystal, (2mm. away) approaching it from the other side. Because the thermocouple could not be coincident with the centre of precession, the camera motion was observed to produce fluctuations in the amount of heat reflected onto it by the layer-line screen. These fluctuations were quite regular and were of an amplitude of up to 2°C at 580°C, the actual size varying with the coil temperature and the crystal to screen distance. Such fluctuations should not have been present at the crystal, since it was at the true centre of the motion. The reference junction of the thermocouple was maintained at 0°C and millivolt readings were recorded on a chart recorder and converted to temperatures

using conversion tables (16).

To avoid changes in crystal temperature due to draughts, the entire camera and beam port were encased in a housing of polyethylene sheeting. Temperatures were regulated by use of a variable transformer, limiting the amount of electric current passing through the coil.

Low Temperature Apparatus:

Low temperatures were achieved by the use of a simple delivery system which passed dry nitrogen through coiled copper tubing which was immersed in liquid nitrogen and hence through a glass dewar tube to the area of the crystal. The nozzle of the dewar was positioned so that the flow of cold N_2 would fall over the crystal and bathe it completely. Rates of flow were measured by a small manometer attached between the gas supply and the cooling coils. The coils were of sufficient length to equilibrate the gas to the same temperature throughout all ranges of pressure used in the experiment (5 - 20 mm Hg.). To prevent formation of frost on the edges of the nozzle, a small heating coil was fitted around the perimeter of the tube. In addition general frosting was reduced by encasing the entire camera and the nozzle end of the delivery tubes in a polyethylene tent and sealed from the room. The atmosphere inside the tent was dried with Silica gel dessicant.

No attempt was made to measure the actual temperature

at the crystal, but the apparatus had been previously calibrated to deliver approximately -150°C for a nominal delivery pressure of 15 mm Hg. This pressure was used during photographic experiments.

CHAPTER IV

CRYSTAL STRUCTURE AND PHASE TRANSFORMATIONS OF $Na_4P_2O_7$

Introduction

Very little detailed crystallographic research has been done on the pyrophosphates of the alkali metals. In 1957, Corbridge (17) compared the space group symmetries and unit cell sizes of certain hydrated pyrophosphates and hypophosphates, noting that the structures of some compounds were insensitive to which anion was present. Since then, Collin and Willis have described the detailed structure of sodium dihydrogen hypophosphate hexahydrate (18) ($Na_2H_2P_2O_6 \cdot 6H_2O$) and Collin has determined the structure of the isomorphous pyrophosphate (18) ($Na_2H_2P_2O_7 \cdot 6H_2O$).

McDonald and Cruickshank (19) have refined the structure of $Na_4P_2O_7 \cdot 10H_2O$, first determined by MacArthur and Beevers (20) in 1957, and have found bond lengths of 1.612(5) Å for the P-O (bridge) bond, 1.523(4) Å for the P-O (outer) bond and a P-O-P bending angle of 130.2°. The orientation of the anion is expected to be affected by the surrounding water molecules and the bond lengths and angles may also be affected. Investigation of the detailed crystal structure of anhydrous $Na_4P_2O_7$ should elucidate the extent of these effects.

Partridge, Hicks and Smith (3) have reported that several apparently reversible phase transformations occur in $Na_4P_2O_7$ when the temperature is raised continuously to the melting point. Five different forms were indicated by a differential thermal analysis and high temperature microscopy. Four of these forms were detectable by changes in the X-ray diffraction pattern of a crystalline sample. The transformations are related in the following way:

$$Na_4P_2O_7\ V \underset{}{\overset{400^\circ}{\rightleftharpoons}} Na_4P_2O_7\ IV \overset{510^\circ}{\rightleftharpoons} Na_4P_2O_7\ III \overset{520^\circ}{\rightleftharpoons} Na_4P_2O_7\ II \overset{545^\circ}{\rightleftharpoons} Na_4P_2O_7\ I \overset{985^\circ}{\rightleftharpoons} \text{Melt.}$$

In this research, single crystals of $Na_4P_2O_7$ were studied and the symmetries of four forms are reported, phase III being undetected, possibly because of uncertainties in the exact temperature of the crystal during high temperature investigations.

During the course of this study, it was determined that the symmetry and thus the indexing of reflections in the powder pattern for $Na_4P_2O_7$ listed in the ASTM files, is erroneous (21). The symmetry is orthorhombic, not hexagonal as reported, although the strong reflections do bear some "pseudo-hexagonal" relationships to each other.

Experiments:

Crystals of anhydrous sodium pyrophosphate were obtained by heating crystals of the decahydrate (Reagent grade) to above

1000°C and then cooling slowly to room temperature. The crystals grew in the form of plates separated by thin layers of microcrystalline material. Crystal density was determined to be 2.50 gm./cc. by flotation in bromoform. The linear absorption coefficient was calculated (μ = 8.75 cm^{-1}) and found to be low enough that size effects could be substantially ignored and crystals were selected for quality alone.

Two crystals were used in the study of the room temperature phase, both of the order of 0.1 mm in length and approximately cube-shaped. The first of these was mounted with the c axis parallel to the rotation axis and Weissenberg photographs were taken of the zeroth, first and second layers of the 001 zone. Intensity data from the hk0, hk1 and hk2 layers were measured using MoKα radiation and the manual scintillation counter as described in Chapter III. Instrument dead-time corrections were not significant.

The crystal was then transferred to a precession camera and integrated photographs of the h0ℓ, h1ℓ, and h2ℓ layers were recorded. The combined effects of high background and alignment problems made the data so collected, of limited use.

Another crystal of similar size was selected and mounted with the c axis parallel to the spindle axis. Photographs of the h0ℓ, h1ℓ and h2ℓ layers recorded with MoKα radiation on a precession camera, were of good quality and the reflection intensities were measured using a microdensitometer. The data

were then corrected for Lorentz and polarization effects and converted to phaseless structure factors.

The investigation of the high temperature phases of sodium pyrophosphate was facilitated by the low linear absorption coefficient of the compound. The use of a large crystal was both practical and desirable. The main advantage was very short exposure times during which high temperatures could be maintained at the crystal without excessive heat damage to the film.

A crystal in the shape of a triangular prism measuring 0.5 mm across the base of the triangle and 1.0 mm. down the length of the bar, was mounted with the spindle axis approximately parallel to the length of the crystal. The crystal was aligned so that the [210] axis served as the rotation axis. The preferred orientation would have been with a principal axis along the spindle, but restrictions were placed on the displacement of the goniometer arcs by the heating coils making such reorientation impractical. In any case, inspection of the room temperature hk0 photograph showed a "pseudo-hexagonal" pattern among the strong spots indicating that the [210] might become a symmetry axis in one of the high temperature phases. An overall suggestion of near C-centering was also noted.

The crystal was photographed at various temperatures ranging from 319°C to 578°C as well as at room temperature.

Temperatures at the crystal remained constant to within 5°C throughout the duration of each exposure; however, the temperature at the crystal may have deviated by 10°C from that at the thermocouple. Thus the phase changes reported at 510°C and 525°C were not resolved within this apparatus. The apparatus and its operation is described in Chapter III. Experimental results are summarized in Table 4.1 and described in more detail below.

Observations of diffraction patterns:

From room temperature to 400°C no change was observed in the diffraction pattern. A systematic extinction pattern was observed as only reflections with even indices appeared along the three axes of an orthorhombic unit cell, with axis lengths:

$$\underline{a} = 9.4\ \text{Å} \quad , \quad \underline{b} = 5.4\ \text{Å} \quad \text{and} \quad \underline{c} = 13.48\ \text{Å} \ .$$

This was consistent with the space group $P2_12_12_1$.

Above 400°C several changes occurred in the diffraction pattern. The "pseudo-centering" noted as a distribution of intense and weak reflections in the room temperature structure, became complete with only h + k = 2n reflections observable. The intensity of the previously unobserved 220 reflection became measurable. Simultaneous with this change the $\underline{c}$ axis doubled in length defining a new unit cell with dimensions $\underline{a}$ = 9.4 Å, $\underline{b}$ = 5.4 Å, and $\underline{c}$ = 26.96 Å. With indices referring to this cell, the 006 and 0014 reflections confirmed both the

TABLE 4.1

Temperature (°C)	Systematic Extinctions	Axis Lengths (Å)	Molecules per unit cell	Space Group
< 375° to 391°	(h00) h≠2n (0k0) k≠2n (00ℓ) ℓ≠2n	a = 9.4 b = 5.4 c = 13.48	4	$P2_12_12_1$
406° to 510°	h+k≠2n (00ℓ) ℓ≠2n	a = 9.4 b = 5.4 c=(13.48)×2 β = 91.5°	8	C2/c or Cc
533° to 556	h+k≠2n (00ℓ) ℓ≠2n	a = 9.4 b = 5.4 c=(13.48)×3	12	$C222_1$
Above 556°	h+k≠2n (00ℓ) ℓ≠2n	(hexagonal) a = 5.4 b = 5.4 c = 13.48	2	$P6_322$

the doubling of the c axis and the retention of the 2_1 symmetry operation along its length. The space group appeared consistent with space group $C222_1$ with 8 molecules per unit cell.

From 406°C to 510°C the intensity of the 220 reflection increased monatonically, while the intensities of the 006 and 0014 reflections decreased uniformly becoming unmeasurable at 510°C.

Between 510°C and 540°C reflections in the 31ℓ and 62ℓ reciprocal lattice rows became ill-defined and tended to merge with one another, suggestive of possible stacking disorders occuring in the structure parallel to the c direction. This effect diminished with rising temperature so that a photograph at 578°C showed no reflections in the 31ℓ lattice row below the 314 reflection (ℓ index referring to c = 13.48 Å). The 314, 315 and 317 reflections were all well defined and strong. At this temperature the orthorhombic symmetry of the hk0 projection had been replaced by a full six-fold symmetry and the c axis length had returned to 13.48 Å, retaining the systematic extinction pattern (00ℓ) $\ell \neq 2n$. Reindexing of the cell in the hexagonal system showed that the symmetry is consistent with the space group $P6_322$ with axes a = 5.4 Å, b = 5.4 Å and c = 13.48 Å defining a unit cell that contains two molecules.

A more complete survey of the system has since been

carried out by K. Y. Leung. By use of a much smaller crystal and a more advanced heating apparatus, data of a much higher quality has been obtained. It has been determined that the transition at 400°C leads in fact, to a monoclinic unit cell of dimensions $\underline{a}$ = 9.367 Å, $\underline{b}$ = 5.390 Å and $\underline{c}$ = 26.96 Å with β = 91.5° and a symmetry consistent with space group C2/c. Because of the small spot shape it was also possible to resolve the streaks appearing between 510°C and 540°C. These are evidence that the $\underline{c}$ axis has tripled its room temperature length and measures 40.65 Å. The symmetry of this phase is now consistent with the space group $C222_1$. The impression of streaks arose from the large spots merging into one another as the spacing between spots on the photographs decreased to less than the diameter of a reflection. Above 578°C the symmetry appears consistently hexagonal in upper layers of the reciprocal lattice that were not observed in the first survey, and the space group seems to be $P6_322$ or a related symmetry group in the highest temperature phase.

Room Temperature Structure:

As a result of a large number of studies of pyrophosphates it is clear that the P_2O_7 group has a number of characteristic features that can be used to help in analysis of the Patterson function. The anion generally has either a nearly eclipsed or a staggered configuration of terminal oxygen atoms with

a mean P-O bond length of 1.54 Å. Bonds to the bridging oxygen are characteristically up to 0.08 Å larger than the mean, and P-O bonds to terminal oxygens can be up to 0.05 Å shorter than this average. The anion is either bent at the bridging oxygen atom or undergoes disorder and a relationship exists between the P-O-P bond angle and the deviation of the bond lengths from the mean such that the P-P distance tends to remain about 3.1 Å. The O-O interactions about any PO_4 tetrahedron are about 2.5 Å in length and represent a considerable contraction relative to the Van der Waals radius of an oxygen atom.

The magnitudes of the various types of Patterson vectors expected to be present in the structure were calculated relative to the peak at the origin and are listed in Table 4.2. The origin peak includes contributions from all interactions within the unit cell, and the magnitude of the peak may be calculated:

$$\begin{aligned} P_{ooo}(\text{calc}) &= Z[4(\rho_{Na})^2 + 2(\rho_p)^2 + 7(\rho_o)^2] \\ &= 4[4(11)^2 + 2(15)^2 + 7(8)^2] \\ &= 5368 \end{aligned}$$

where Z is the number of molecules per unit cell, and ρ_A is the number of electrons residing on atom A. The relative magnitude of an interaction between atoms A and B is given by:

$$\frac{\rho_A \times \rho_B}{5368} .$$

The (u,v) projection of the Patterson function (Fig. 4.1) showed a great deal of superposition of Patterson vectors along

TABLE 4.2

Patterson Vector	Magnitude relative to P_{ooo}
P-P	.042
Na-P	.031
Na-Na	.023
P-O	.023
Na-O	.016
O-O	.012

Figure 4.1

The (u,v) projection of the Patterson function of $Na_4P_2O_7$. Contour lines have been drawn at increments of $1/8 \times P_{oo}$ for values between $\frac{1}{4}$ and $\frac{3}{4}$ of the origin peak. For clarity, no controus of lower value were drawn but peak positions were marked with the symbol +. The adjacent number indicates the peak height relative to the origin. Many peaks were elongated in the u direction and the symbol +—+ marks the area of maximum intensity. The asymmetric zone is $\frac{1}{4}$ of the full diagram.

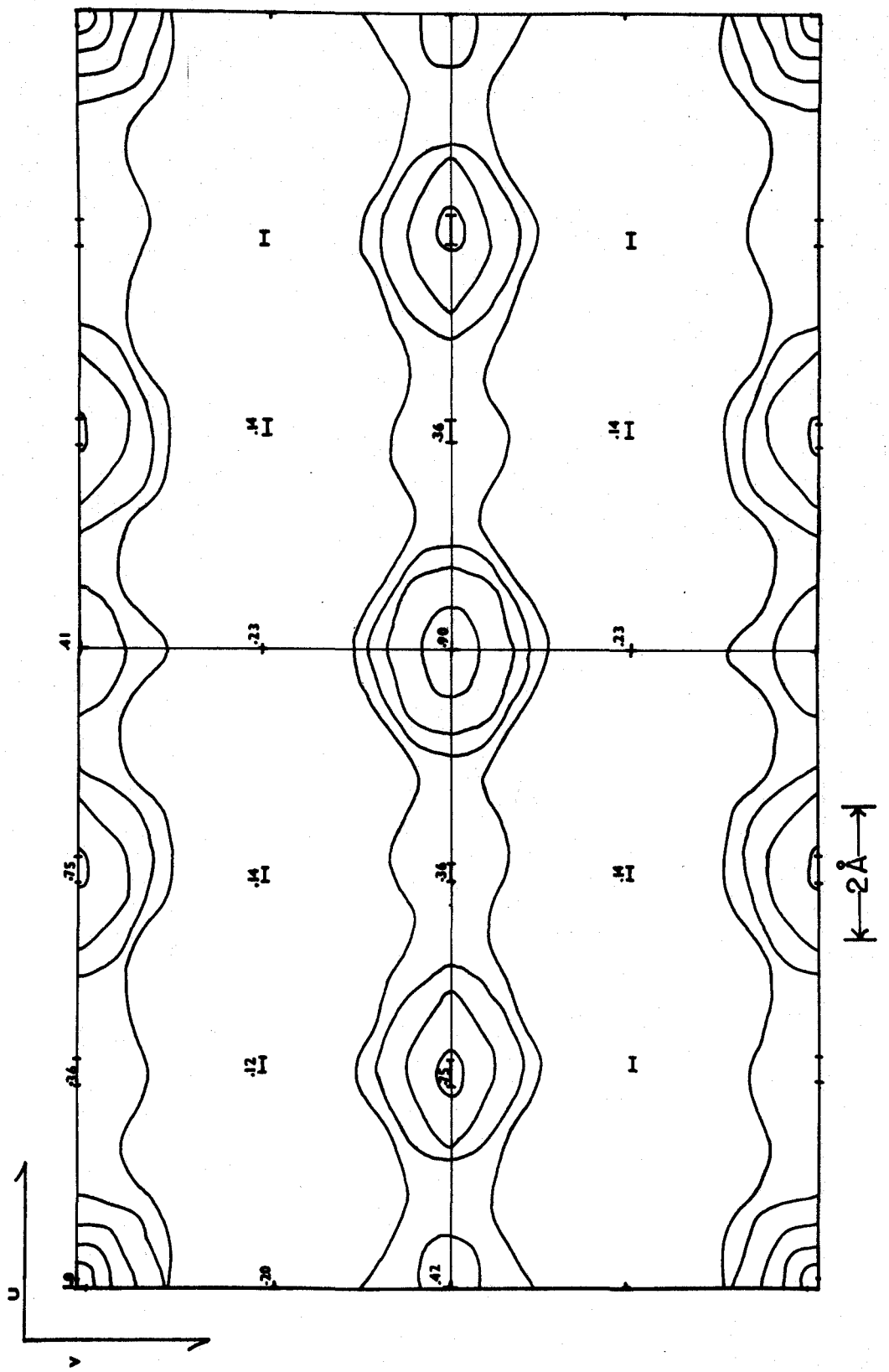
U
V
2Å

Figure 4.2

The (u,w) projection of the Patterson function of $Na_4P_2O_7$. Contour lines occur in increments of $\frac{1}{8} \times P_{oo}$ for values between $\frac{1}{4}$ and $\frac{3}{4}$ of the origin peak. Peak positions are represented by the symbol + for symmetrical maxima and by +—+ for maxima elongated along $\underline{u}$. The asymmetric zone is $\frac{1}{4}$ of the full diagram.

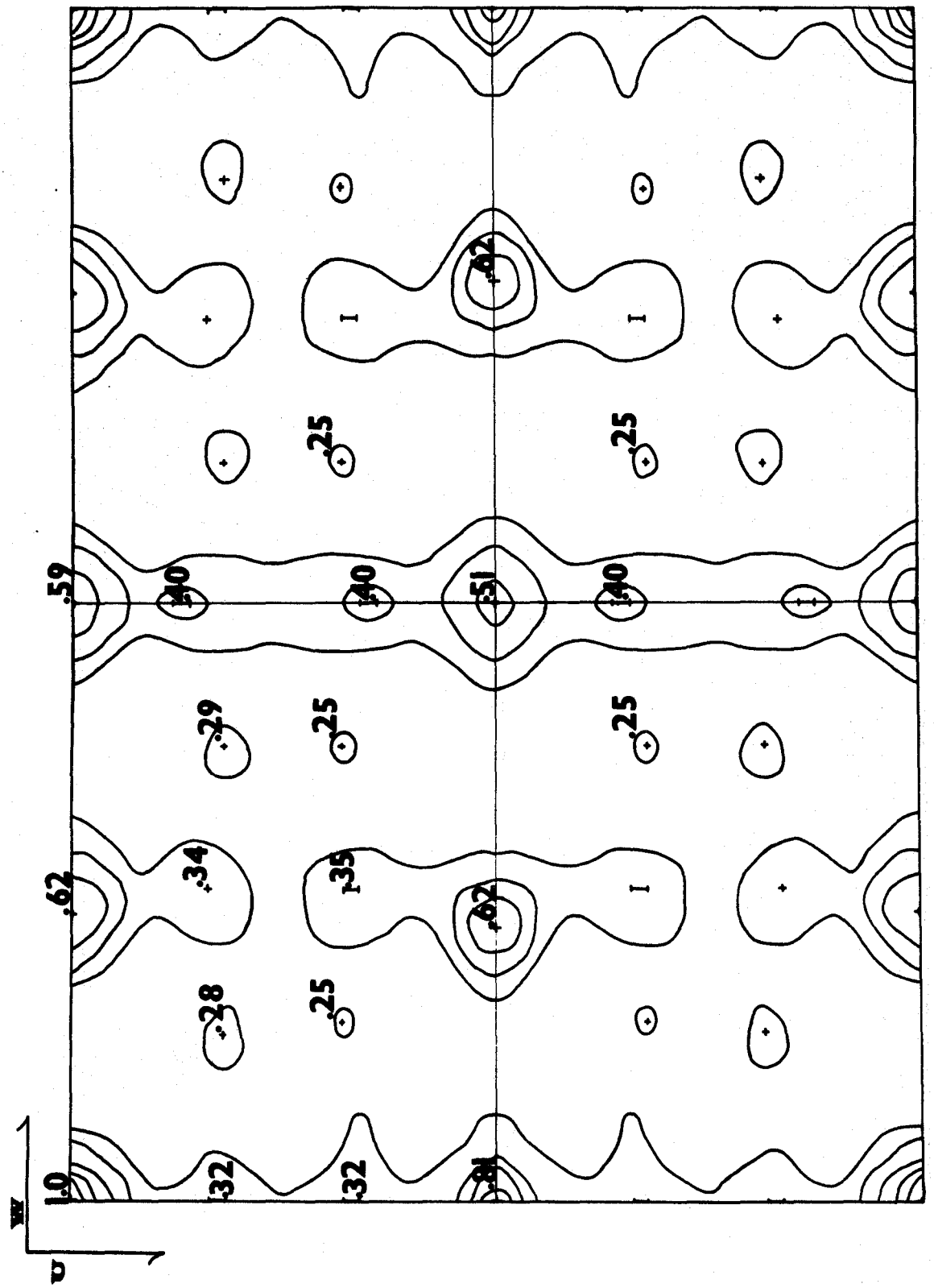
.59
.62
1.0
.40
.40
.51
.40
.25
.25
.25
.25
.29
.34
.35
.62
.28
.25
.32
.32
.91
.62
I
I
I
W
b

the lines v = 0 and v = $\frac{1}{2}$. Peaks of about 0.75 the magnitude of the origin peak were situated at $(\frac{2}{3},0)$ and at $(\frac{1}{3},\frac{1}{2})$ indicated a "pseudo-hexagonal" relationship existed among the heavy scatterers in the unit cell when projected on the (x,y) plane. A stronger peak (.90 × P_{ooo} at $(\frac{1}{2},\frac{1}{2})$ indicated a large tendency towards C-centering existed in the structure.

When the dimensions of the unit cell were considered, along with the fact that at least the (x,y) projection of the structure attained six-fold symmetry via a series of apparently reversible phase transitions, it became apparent that a structure consistent with the Patterson function could be described by a chain of two pyrophosphate anions parallel to the c axis at $(\frac{1}{4},0)$ in the (x,y) projection and another at $(\frac{3}{4},\frac{1}{2})$. Since these are general positions, the coordinates of all four formula units were fixed by the determination of the coordinates of one.

The cell dimensions in the (x,y) plane are very suggestive of layers of close-packed oxygen atoms. In particular, the 5.4 Å axis is almost a multiple of the diameter of an oxygen atom. If two oxygen atoms are situated with the line between their centres parallel to the b axis and the third terminal oxygen is centred on the a axis, the configuration shown in Fig. 5.3 is produced. This arrangement produces a hole of slightly larger diameter than that corresponding to a close-packed oxygen atom centred on $(\frac{1}{2} - x, \frac{1}{2})$ where $x \simeq 0.1$.

If the pyrophosphate anion has an eclipsed arrangement of terminal oxygen atoms, the space group symmetry requires that the next layer be staggered. This has the effect of shifting the hole from $(\frac{1}{2} - x, \frac{1}{2})$ to $(x, \frac{1}{2})$. Thus two sets of two columns are produced in the cell. The hk0 Patterson function is consistent with atoms at these sites but the magnitude of peaks at (.32,0) and (.18,.50) indicates rather more superposition of vectors than the model predicts. It is found that each anion is surrounded by three columns. Each column can only contain two sodium atoms. Assuming all Na atoms are in columns each molecule has $6 \times \frac{1}{3}$ sodium atoms, which does not satisfy the stoichiometry of the compound.

If the anion has staggered terminal oxygen atoms, the "empty" column is shifted by one-half the length of the anion in the c direction.

Since the sodium positions satisfy the (u,v) Patterson projection, an arrangement of oxygen atoms was sought that would allow all four of the sites to be occupied by sodium ions on the same level in the cell, providing $12 \times \frac{1}{3}$ cations for each anion and thus satisfy the stoichiometry of the compound. The most satisfactory arrangement is shown in Fig. 4.4. The oxygen atoms are not strictly close-packed in the layer, but do leave vacant sites at $(x,\frac{1}{2})$, $(\frac{1}{2} -x,\frac{1}{2})$, $(\frac{1}{2} + x,0)$ and $(\bar{x},0)$. Since these are symmetry related positions, the determination of the coordinates of one Na atom will give the position of one in each of four related sites. As in the close-packed model,

Figure 4.3

A section of the unit cell of $Na_4P_2O_7$ parallel to the ab plane. The cross-hatched circles represent centres of holes produced by terminal oxygen atoms of pyrophosphate anions in one layer only. The black circles represent the positions of phosphorous atoms in this model.

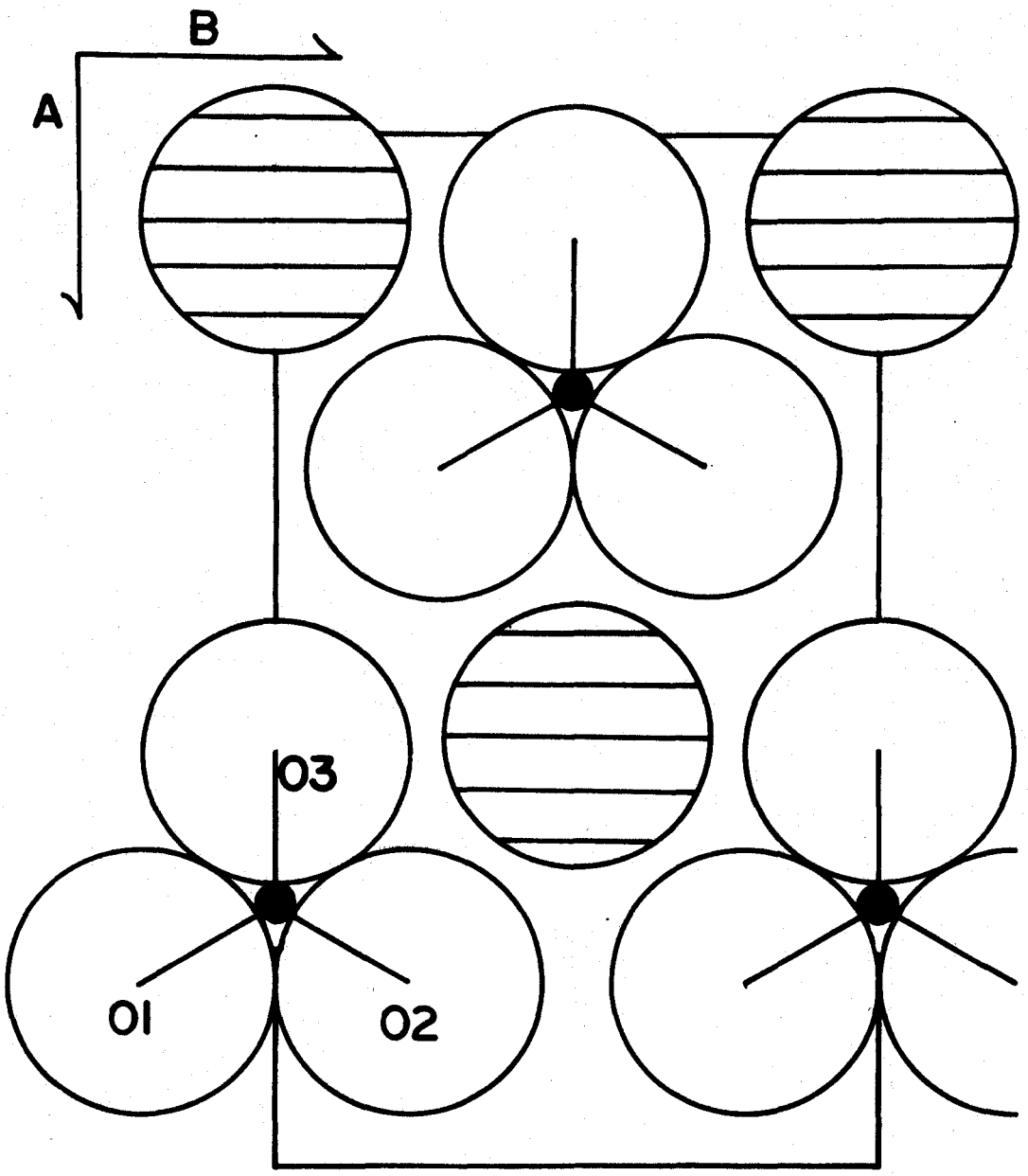
B
A
03
01
02

symmetry requires that the next layer be staggered. Fig. 4.5 shows that this arrangement produces vacancies centered on the same positions as in Fig. 4.4. Thus "vacant" columns parallel to the c direction extend throughout the length of the unit cell. In this preliminary model it is assumed that the pyrophosphate anion has a central P-O-P bond angle of 180°. Each anion is surrounded by six identical columns of cations, and so fulfills the six-fold symmetry observed in the highest temperature phase. The two remaining problems are to ascertain the positions of the sodium ions with respect to their Z coordinates and to find the appropriate deviation from the six-fold symmetry that gives rise to the orthorhombic symmetry $P2_12_12_1$.

Rigorous close packing of the oxygen atoms in this arrangement requires that the bond lengths between oxygen atoms and the cation in the octahedral sites be 2.0 Å and in the tetrahedral sites, here occupied by phosphorous, be 1.7 Å. However, 1.7 Å is unusually long for a P-O bond, the preferred distance being 1.54 Å. Since the terminal oxygen atoms do not lie in a line between the Na and P positions, this shorter bond distance can be achieved by a rotation of the triangle of oxygen about the sodium ion, in the direction of the phosphorous site. Such a rotation, when followed by a very slight translation increases the Na-O bond length to 2.13 Å while the new P-O distances are very close to 1.5 Å. If the anion is in a staggered

Figure 4.4

A section of the $Na_4P_2O_7$ unit cell parallel to the ab plane. Only one set of terminal oxygen atoms is represented. The black circles indicate the positions of the phosphorous atoms to which the oxygens are bonded. The cross-hatched circles represent the centres of holes produced by sets of three oxygen atoms whose centres are related by equilateral triangles.

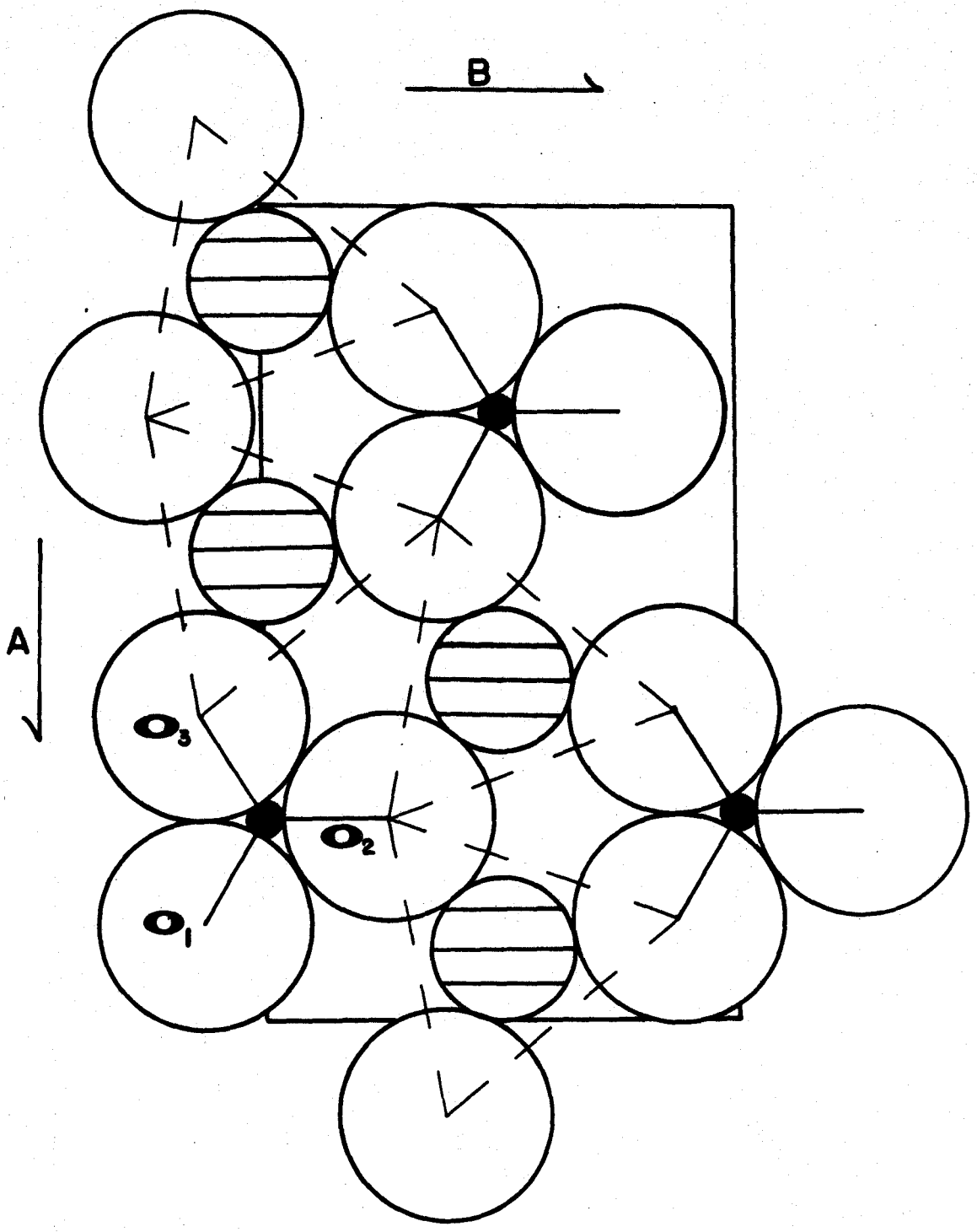
B
A
O3
O2
O1

Figure 4.5

A section of the $Na_4P_2O_7$ unit cell parallel to the ab plane. The plane containing oxygen atoms adjacent to the plane in figure 4.4 is represented, separated from that plane by approximately 2.4 Å along c. Although this layer of oxygen atoms is staggered with respect to the last, the holes produced are centred on the same positions.

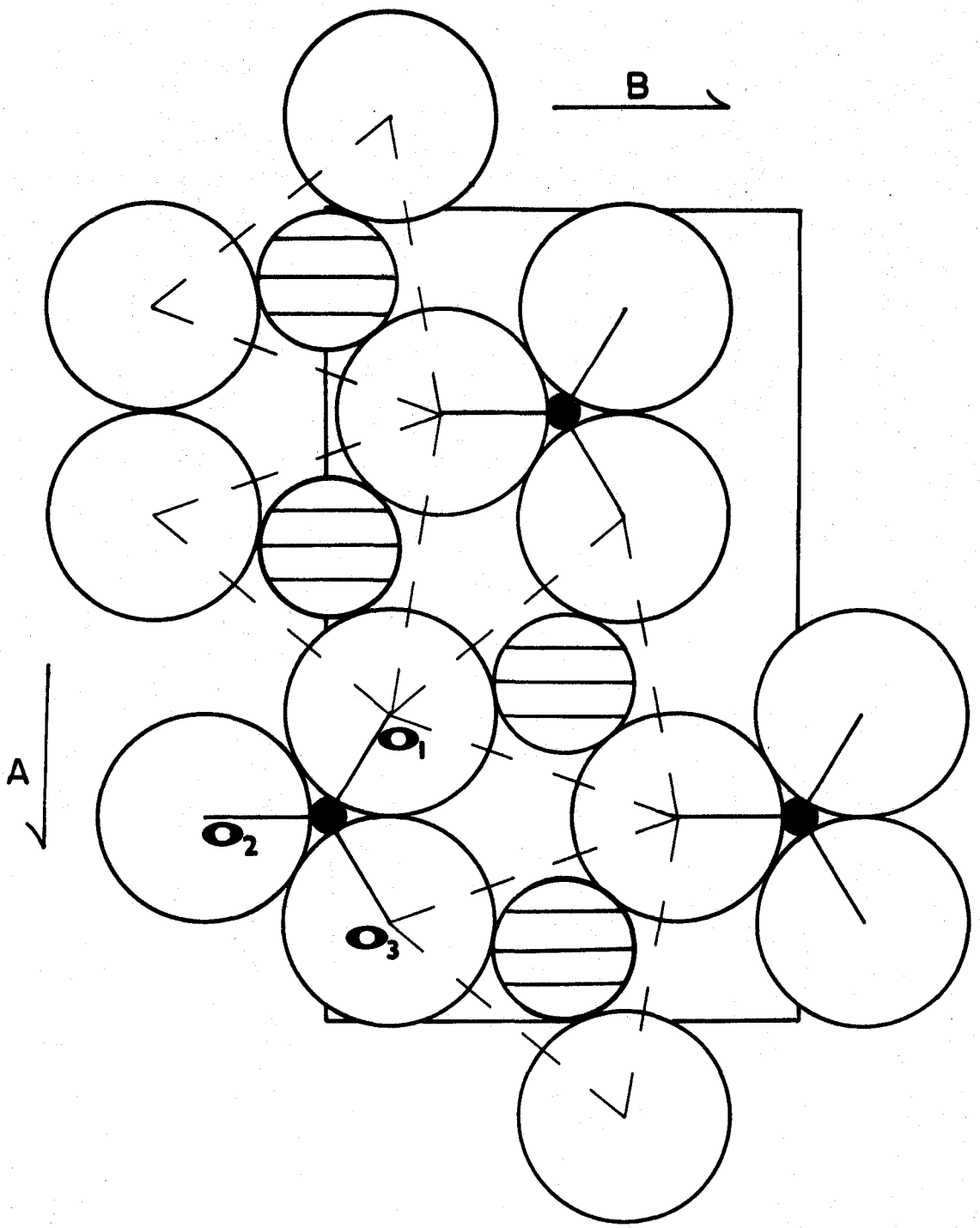
B
A
O1
O2
O3

conformation, the next layer of oxygen atoms will superimpose exactly on the first layer. If the anion is in the eclipsed configuration, the next layer will be staggered with respect to the first and the triangle of oxygens will undergo a similar planar rotation, but in the opposite sense. This produces a slightly distorted octahedral site which a sodium ion can occupy with bond lengths of $\sim$ 2.13 Å to all six oxygen atoms. Figure 4.6 illustrates this environment.

The difficulty with this model, however, is in finding a position for the second sodium along c in the column. The best site in terms of coordination is at the same level as the bridging oxygen atom in the pyrophosphate anion. This gives a symmetrical nine-fold coordination with Na-O bond lengths of $\sim$ 3.1 Å to the three bridging oxygens and $\sim$ 3.24 Å to the six terminal oxygen atoms. These bond lengths are much longer than typical sodium-oxygen bonds. Thus, some distortion must occur in the pyro group such that oxygen atoms will approach the centre of this site. If the bridging oxygen of one anion were advanced toward the sodium atom, a bend in the P-O-P bond would result. Such a bending is typical of pyrophosphate structures. $Na_4P_2O_7 \cdot 10H_2O$ is reported by Cruickshank (19) to have a P-O-P angle of 130°. If the bridging oxygen atom at (.25,0) is advanced toward the sodium atom at (.40,.50) by 0.7 Å, to make a bond distance of 2.4 Å the P-O-P bridging angle would be 126°. Since the oxygen environment is expected to remain tetrahedral with respect to phosphorous, the planes

Figure 4.6

This figure represents a superposition of figures 4.4 and 4.5 and indicates the slightly distorted octahedral hole, formed by the two adjacent layers of oxygen atoms, in which a sodium ion may reside. The black circles represent the positions of the phosphorous atoms which lie above the upper layer of oxygen atoms and below the lower layer. The octahedral site between the close packed oxygen atoms and below the upper phosphorous atom is vacant in this model.

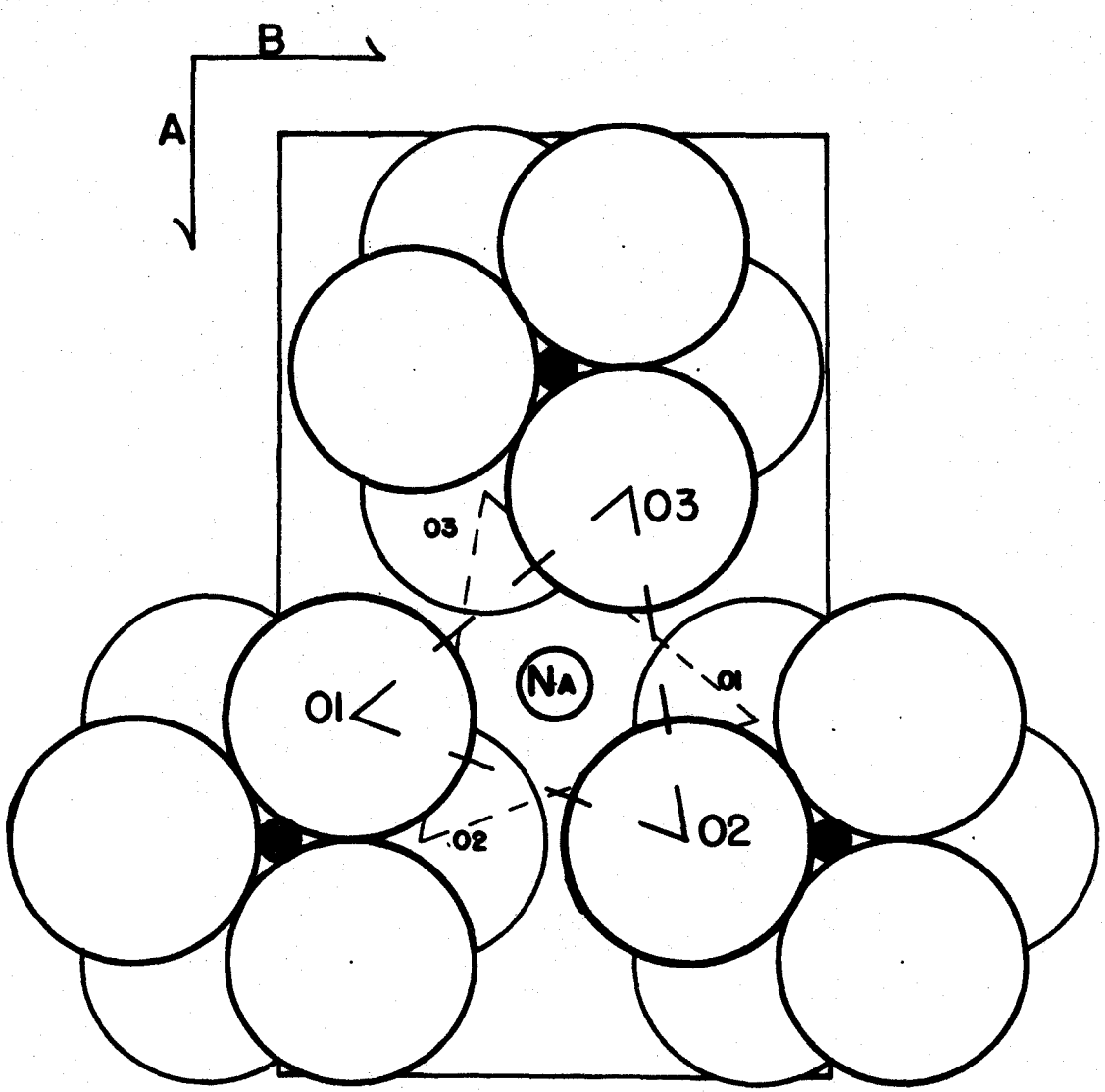
B
A
O3
O3
O1
NA
O1
O2
O2

defined by the terminal oxygens at each end of the anion will be tilted by about 26° to the (x,y) plane, bringing two atoms closer from the top and two atoms closer from the bottom of neighboring anions, while the terminal oxygens at each end of the anion at (.25,0) bend away. The result of such an operation would be 5-fold coordination of the sodium ion nearest to the bridging oxygen atom of the pyro group and a rotated, but still octahedral environment for the sodium ion lying between anions. Least squares refinement of this model with the available data was attempted. The hk0 projection data refined to give a preliminary agreement factor of R = .29.

Fixing the Z coordinates of the atoms proved very troublesome. The h0ℓ and 0kℓ projections of the Patterson function both showed large peaks along the u = 0 and v = 0 lines, separated by about 1.9 Å and 3.2 Å, and similar columns of peaks were distributed along u = .18, u = .34 and v = .50. Problems in resolving superposition of peaks were apparent. From table 4.2, it can be seen that one Na-Na vector contributes exactly the same amount to the Patterson function as one P-O vector. The strongest interactions present are the P-P vectors. Each should contribute 4% of the origin peak and if all symmetry related interactions are taken into account, a peak with intensity 16% of the origin peak should appear. In the (u,w) projection of the Patterson function (Fig. 4.2), no peak is less than 25% of the origin peak. The only clear information derivable from the Patterson function is that most heavy scatterers in

TABLE 4.3 Atomic Parameters for $Na_4P_2O_7$

Atom	X	Y	Z	U_{11}	U_{22}	U_{33}	U_{12}	U_{13}	U_{23}
Na(1)	0.4724(1)	0.4991(2)	-0.01674(6)	0.0150(5)	0.0143(4)	0.0166(4)	0.0010(4)	-0.0005(3)	0.0008(4
Na(2)	0.4919(1)	0.4847(2)	0.23605(7)	0.0198(5)	0.0194(5)	0.0181(4)	-0.0032(4)	0.0058(3)	-0.0018(4
Na(3)	0.1221(1)	0.4960(2)	0.15457(7)	0.0165(5)	0.0195(4)	0.0178(4)	0.0003(4)	0.0020(3)	-0.0020(4
Na(4)	0.6653(1)	-0.0367(2)	0.16745(7)	0.0161(5)	0.0166(4)	0.0210(4)	-0.0014(4)	0.0007(4)	-0.0002(4
P(A)	0.30700(6)	0.0112(1)	-0.10607(4)	0.0088(2)	0.0090(2)	0.0081(2)	-0.000(2)	-0.0000(2)	0.0001(2
P(B)	0.31379(6)	-0.0224(1)	0.11128(4)	0.0090(2)	0.0100(2)	0.0083(2)	-0.0004(2)	0.0005(2)	-0.0001(2
OCE	0.3601(2)	0.0972(3)	0.0041(1)	0.0148(8)	0.0135(6)	0.0079(6)	-0.0049(6)	-0.0002(5)	-0.0000(6
OA3	0.1491(2)	-0.0448(4)	-0.1020(1)	0.0089(8)	0.0278(9)	0.0145(7)	-0.0017(6)	-0.0002(5)	-0.0038(7
OA2	0.3952(2)	-0.2132(3)	-0.1338(1)	0.0181(9)	0.0116(7)	0.0141(7)	0.0048(6)	0.0021(6)	-0.0015(6
OA1	0.3442(2)	0.2338(3)	-0.1693(1)	0.0250(10)	0.0115(7)	0.0136(7)	0.0002(6)	0.0008(6)	0.0056(6
OB2	0.3204(2)	-0.3018(3)	0.1008(1)	0.0208(9)	0.0094(6)	0.0208(8)	-0.0008(6)	0.0061(7)	0.0001(6
OB1	0.4265(2)	0.0801(4)	0.1805(1)	0.0125(8)	0.0239(8)	0.0122(7)	-0.0030(7)	-0.0039(5)	-0.0024(6
OB3	0.1654(2)	0.0732(3)	0.1334(1)	0.0105(8)	0.0195(7)	0.0148(7)	0.0018(6)	0.0030(5)	-0.0024(6

U_{ij}'s in $\mathring{A}^2$ are computed from $\beta_{ij} = 2\pi^2 \underline{b}_i b_j U_{ij}$ where $T = \exp\{-[\beta_{11}h^2 + 2\beta_{12}hk+...]\}$appears in the structure factor expression and b_j are reciprocal lattice vectors.

Refined unit cell parameters: $\underline{a}$ = 9.367(5), $\underline{b}$ = 5.390(2), $\underline{c}$ = 13.480(8).

the cell are separated by 3.2 Å in Z as indicated by the strong (62%) peak at u = 0, w = .25.

If the model structure was correct, vectors between columns of sodium atoms should have contributed at u = .30 and have extended along w. These were observed at u = .33. A similar column was expected along w at u = .20 and, in agreement with the shift above, the column was observed at u =.17. Unfortunately, the vectors representing interactions between a sodium column and a pyro anion should have occurred along w at $u = .25 + \frac{.17}{2} = .34$. Thus, these interactions are superimposed on the Na-Na interactions. A similar effect was observed at u = .17.

Subsequent attempts at analysis of the structure included use of Patterson sections of both (u,v) and (v,w) planes and spaced about 1 Å apart. This approach also failed to resolve the problems presented by superposition of the interatomic vectors, and the structure was not resolved by these techniques.

A later attempt by K. Y. Leung to solve the room temperature structure was successful. Using both film data and data collected by a Syntex automatic diffractometer, the structure was solved by direct methods, thus avoiding the problems presented by the Patterson function. The methods employed were based on the theory developed by Hauptmann and Karle (22) and followed the example worked for the $P2_12_12_1$ space group by I. Karle (23). The atomic positions and refined lattice parameters are presented in Table 4.3 and a diagram of the (x,y)

projection of the structure is presented in Fig. 4.7.

Discussion:

It is interesting to compare the refined structure and the model developed from packing arguments and analysis of the Patterson function,particularly in reference to the (x,y) projection of the structure, for which a reasonable degree of agreement existed between the data and the model. The basic difference between the two structures lies in the choice of origin. To illustrate this, the (x,y) projection of the proposed model shows two anions lying parallel to Z at $(\frac{1}{4},0)$ and two at $(\frac{3}{4},0)$. Columns of sodium ions lie parallel to Z at $(.40,\frac{1}{2})$ and at symmetry related positions. Fig. 4.8A represents the positions (in fractional coordinates), of the atoms in the refined structure plotted using the same origin as the proposed model. One finds a column of four Na ions centred on (.4,0) but with slightly different x coordinates. Two pyro anions are found close to $(\frac{1}{4},0)$ but again have differing x coordinates. Figure 4.8B shows the similar projection of the refined structure using the correct origin. It is obvious that a labelling problem existed in the earlier model. If the phosphorous and sodium atoms are considered as heavy scatterers

Figure 4.7

The diagram shows the refined structure of $Na_4P_2O_7$ viewed down the 13 Å axis and illustrates the hexagonal nature of the (x,y) projection of the structure. The diagram is reproduced by courtesy of K. Y. Leung.

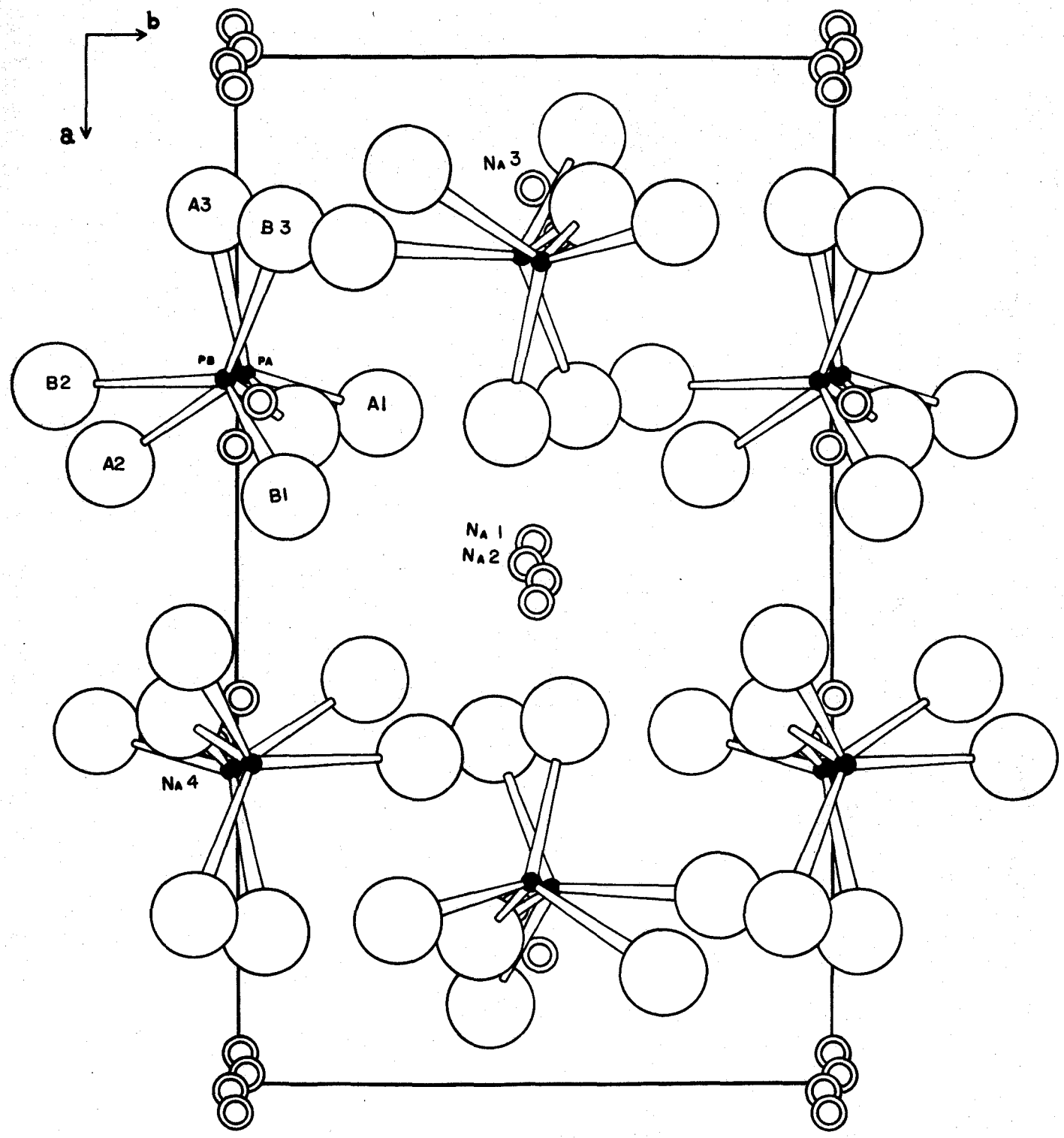
b
a
NA 3
A3
B 3
PB
PA
B2
A1
A2
B1
NA 1
NA 2
NA 4

Figure 4.8

The (x,y) projection of the $Na_4P_2O_7$ unit cell. The diagrams compare the effect of choice of origin on the positions of the relatively heavy scatterers in the unit cell. Only the phosphorous atoms (cross-hatched spheres) are represented from each pyrophosphate anion. Symmetry elements are marked with the symbolism used in the International Tables (34).

Figure 4.8A shows the origin chosen for the proposed model and 4.8B is drawn with the origin consistent with the refined structure.

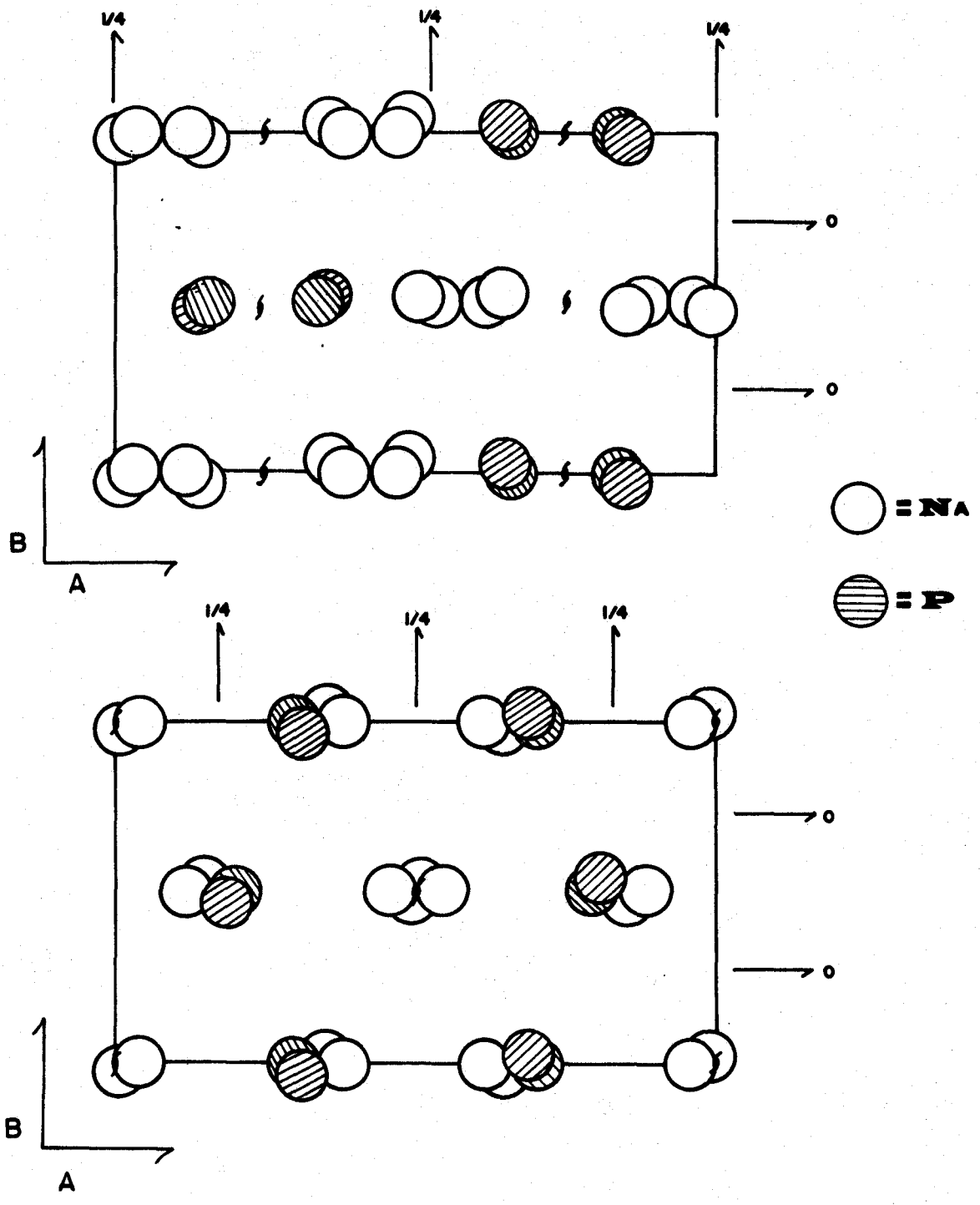
1/4
1/4
1/4
0
0
B
A
= Na
= P
1/4
1/4
1/4
0
0
B
A

of approximately equal weight, the similarity between the projections is large. Groups of four atoms occur $\frac{1}{4}$ apart in x along y = 0 and y = $\frac{1}{2}$, with the groups along y = $\frac{1}{2}$ being shifted by $\frac{1}{8}$ x with respect to the groups along y = 0.

The similarities between the proposed model and the refined structure were sufficient to give a relatively good agreement between calculated and observed structure factors and produced unwarranted confidence in the proposed structure. The choice of origin was also influenced by the ease with which the structure adapted to the $P6_322$ symmetry that was indicated for the highest temperature phase. The pseudo-hexagonal symmetry was very easy to generate with the proposed model and is in part indicated by the intensity distribution of reflections in the room temperature phase. The relatively smooth appearance of the several transitions at higher temperatures, culminating in an apparently hexagonal structure, also led to confidence in the "chain-like" arrangement of species in the structure. The only change required was an apparent straightening of the sodium chains along the c direction, a similar straightening of the P-O-P bond in each anion and a rotation of terminal oxygen atoms.

Discussion of Phase Transformations:

The actual mechanisms of the transitions in symmetry with increasing temperature are not yet clear. However, several features of the transitions can be deduced from the room temperature structure if a simplified model is considered.

The refined structure of $Na_4P_2O_7$ at 22°C can be described as deviant from a simple "idealized" structure. The model consists of pairs of PO_4^{3-} tetrahedra sharing a bridging oxygen colinear with the phosphorous atoms and the P-O-P vector lying parallel to the c axis. The terminal oxygen atoms are eclipsed when viewed down this vector. The anions occur in layers such that the bridging oxygen atoms in a layer lie on a plane perpendicular to c and any three mutual neighbors form an equilateral triangle with the Na^+ ion, Na(1), at the centroid. In the succeeding layer, the triangle formed by neighbouring bridging oxygen atoms is rotated by 60° in the plane, forming an octahedral pattern when considered with the triangle in the layer below. As well as a Na^+ ion at each centroid, a second kind of Na^+ ion, Na(2), lies colinear with the first along c. This cation is octahedrally coordinated between layers to the terminal oxygen atoms from six pyrophosphate anions, three from each layer. Two additional sodium ions, Na(3) and Na(4) are colinear with the P-P vectors and separate the anions in adjacent layers along the c axis.

In this model, the Na(1)-O distances found in the nine coordinate site are quite large (2.7 Å to a terminal oxygen atom and 3.1 Å to a bridging oxygen). This situation can be relieved by a bending of the P-O-P bond such that the bridging oxygen moves toward a sodium ion in one of the 3 surrounding chains. For each choice of direction, the symmetry of the

crystal imposes different restrictions both within the layer and in succeeding layers. Since the PO_4^{3-} groups remain as distorted tetrahedra, the subsequent effects of the sympathetic bending of terminal oxygens can be quite large. The P-O-P bending angle is found to be 127.6° at 22°C. This corresponds to a translation of 0.73 Å by the bridging oxygen from its position in the linear model, toward the sodium ion Na(1). The Na(1)-O bond distances are now quite typical. The bridging oxygen is within 2.43 Å, and on each of the other two anions, one terminal oxygen atom has moved closer as a result of the bending away of the bridging oxygen in their respective anions. In the model, they are predicted to lie symmetrically about the sodium ion, but due to small displacements in the refined structure, the top oxygens from Na-O bonds of 2.31 Å and 2.33 Å and the bottom oxygens remain 2.39 Å and 2.42 Å away. The octahedral site between the layers which is occupied by Na(2) is slightly distorted, showing Na-O bond lengths of 2.35, 2.39 and 2.68 Å with the upper layer and 2.35, 2.51 and 2.52 Å with the lower layer of terminal oxygen atoms.

Figure 4.9 illustrates the (x,y) projection of one half-layer of the idealized model. For convenience of notation, the pyrophosphate anions in the layer within the unit cell are labelled "1" and "2" but are related crystallographically. The terminal oxygen atoms are eclipsed in each anion and can be identified as A, B, or C with C lying in projection along the

a axis and A and B lying to the right and left of the a axis respectively. In the layer above, the anions are again related by a three-fold axis about the chain of Na^+ ions, but as shown in Figure 4.10, the 2_1 axis lying at $(\frac{1}{2},0)$ on the diagram has caused a rotation of the terminal oxygens by 180°. To distinguish this layer from the layer 6.75 Å below, the terminal oxygens are labelled $\bar{A}$, $\bar{B}$ and $\bar{C}$ such that $\bar{A}$ lies to the left of a, $\bar{C}$ lies along a and $\bar{B}$ lies to the right.

The projected P-O bond direction defines a direction along which the bridging oxygen atom may be expected to move, to produce a bend in the anion, destroying the three-fold symmetry in each layer and changing the coordination of the Na^+ ion on the same level. Thus, the notation (AA) describes a layer in which all molecules have the bridging oxygen bent along the line (in projection) of the P-O(A) bond. (AB) represents the configuration in which molecule "1" is bent towards A and molecule "2" is bent toward B. This is sufficient to describe the orientation of all the molecules in the layer. The next layer along c can be described in a similar way, bearing in mind the labelling of the oxygen positions in that layer. Each layer extends approximately 6.75 Å along c.

At room temperature, the crystal has the orthorhombic symmetry $P2_12_12_1$. This imposes the following restrictions on the model. If molecule "1" bends toward A, the bending in

Figure 4.9

The diagram illustrates the projection of a layer of thickness $\underline{c}/4$ of the idealized $Na_4P_2O_7$ structure. Molecules denoted as "1" and "2" are distinct but are related crystallographically. Terminal oxygen atoms are labelled A, B and C and define a possible direction of bending for the bridging oxygen atom of the anion. The bridging oxygen atoms are represented by open circles and lie superimposed in the diagram on phosphorous atoms to which the sets of four oxygens are bonded. Sodium ions on the same level as the bridging oxygen are shown as double circles while sodium ions in the layer but at a lower level are indicated by crosses. The ions at the latter positions are not involved in this discussion. Arrows indicate bending of the bridging oxygen in the direction described as (AA) in the layer.

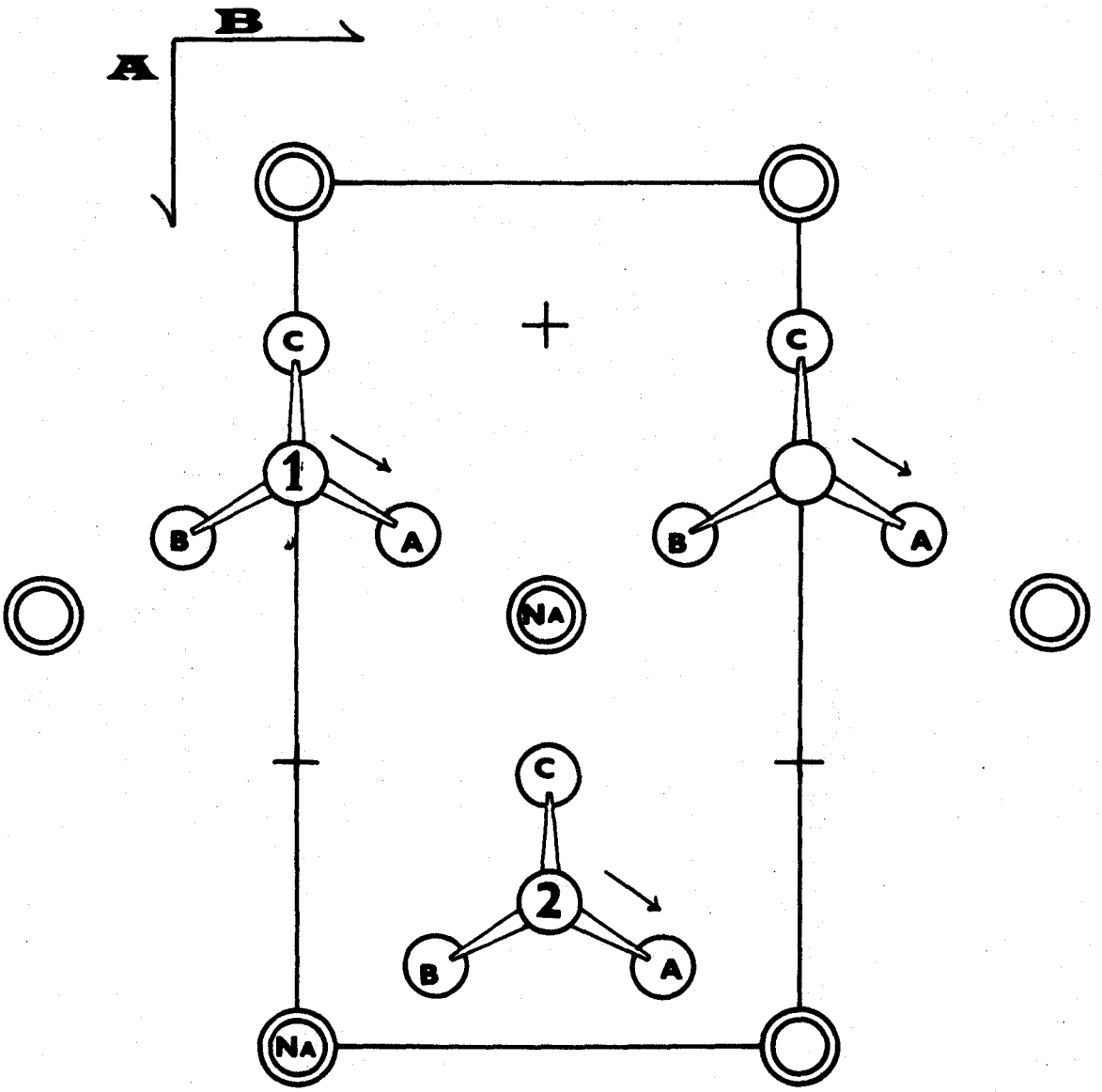
B
A
C
1
B
A
C
B
A
NA
C
2
B
A
NA

Figure 4.10

This figure represents the projection of a layer of thickness $\underline{c}/4$ of the idealized $Na_4P_2O_7$ structure, separated by $\frac{1}{2}\ \underline{c}$ from the layer in Figure 4.9. Here, the labels on the terminal oxygen atoms are $\bar{A}$, $\bar{B}$ and $\bar{C}$. All other notation is consistent with the previous figure. The bending of the bridging oxygen atoms as indicated by the arrows is denoted as $(\bar{A}\bar{A})$.

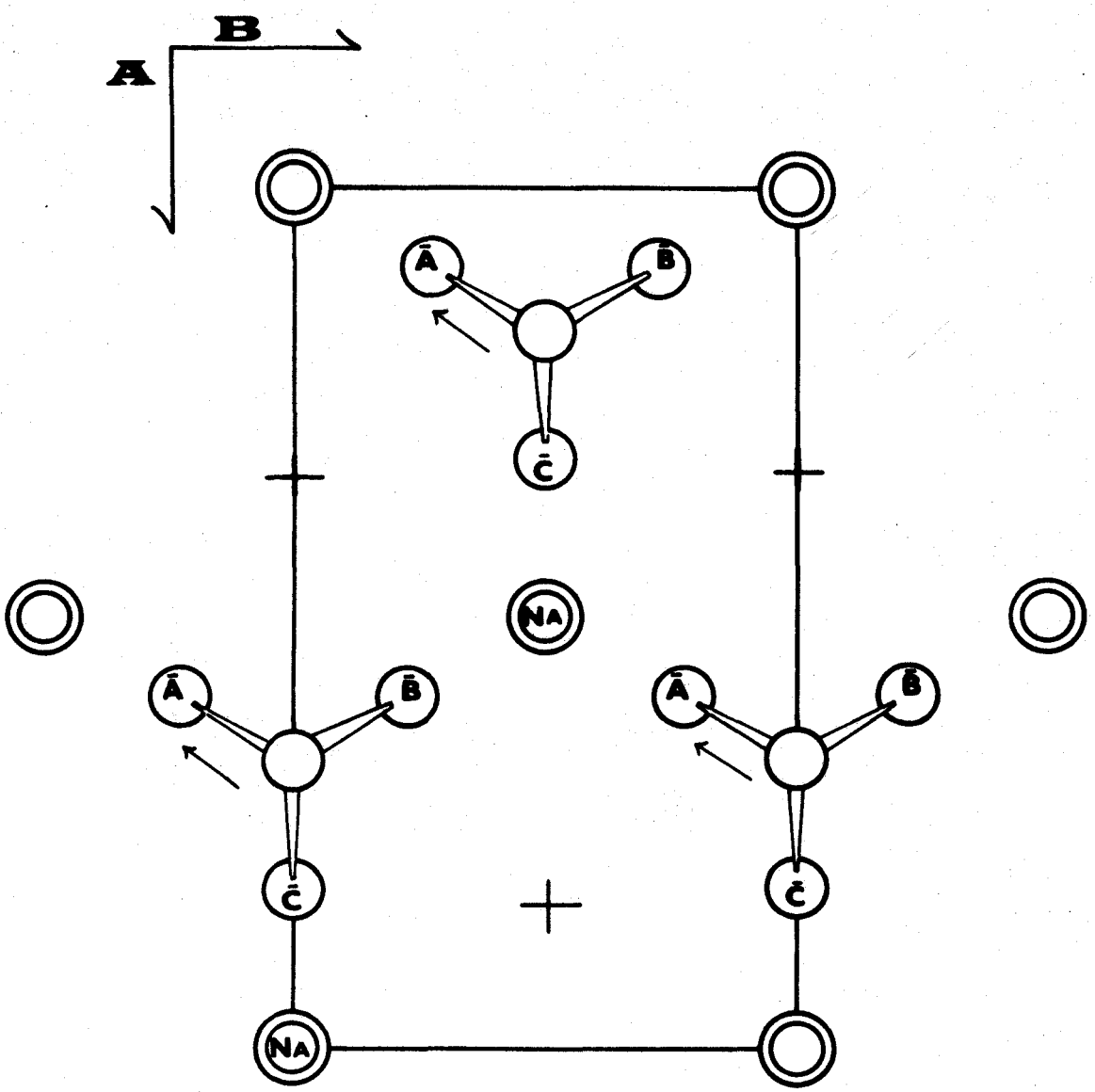
B
A
Ā
B̄
C̄
NA
Ā
B̄
C̄
Ā
B̄
C̄
NA

the layers is restricted to (AB)($\bar{B}\bar{A}$)(AB)($\bar{B}\bar{A}$) .... with two layers defining the repeat distance along c. The bending of molecule "1" along B gives the crystallographically equivalent configuration (BA)($\bar{A}\bar{B}$)(BA)($\bar{A}\bar{B}$) ... . If molecule "1" bends along C, the "C-centred" configuration (CC)($\bar{C}\bar{C}$)(CC)($\bar{C}\bar{C}$) is produced with two layers again defining the unit cell length along c. "C-centering" is not observed in the room temperature structure and the model is limited to the (AB)($\bar{B}\bar{A}$) bending configuration. This bending is observed in the refined structure.

It should be emphasized that this description is a first-order approximation only, and carries with it the assumption that the only deviation from the idealized structure results from the bending of the anion. If an additional distortion occurs, the restrictions on the modes of bending may change. For example, the C-centering predicted by the bending mode (CC) may be destroyed by movement of say the Na^+ ions in the unit cell and the restriction placed on that mode by the symmetry observed at room temperature would not exist. Since the model is based on the room temperature structure, the assumption is justified in this case. In discussion of the higher temperature phases, the justification for the assumption is the apparent ease of the phase transitions and that the dimensions of the original unit cell are essentially unchanged in x and y, and changes which occur in the repeat distance along z are

multiples of the original c axis length, indicating small adjustments destroying the translational symmetry in one direction only.

Above 400°C, the crystal adopts a new symmetry consistent with the symmetries of either the Cc or C2/c space group. Since this involves C-centering, the only bending configurations available for a layer are (AA), (BB) or (CC). In the last case, the bending indicated for succeeding layers is also (CC) so that the crystal would have the configuration (CC)($\bar{C}\bar{C}$) (CC)($\bar{C}\bar{C}$) .... . If no other changes occur in the structure, the length of the unit cell in z would be defined by two layers and c = 13.5 Å. It is observed experimentally that the c axis length is 27 Å. If the assumptions are correct, this bending mode is inconsistent with the observed properties of the structure.

If the bending mode is (AA) in one layer, then two layers above, the bending must be (BB). This indicates a configuration of (AA)(XX)(BB)(X*X*)(AA) .... where X = $\bar{A}$, $\bar{B}$ or $\bar{C}$ and X* is the conjugate such that A* = B, B* = A and C* = C. Every fourth layer is translationally equivalent, requiring a unit cell in which c = 27 Å. If X = $\bar{B}$, the bending configuration produced is crystallographically equivalent to the configuration for X = $\bar{A}$, thus there are only two unique possibilities for the bending arrangement.

The space group C2/c has symmetry which is incompatible with the configuration produced when X = $\bar{C}$, since neighboring

layers must be related either by a two-fold axis or a centre of symmetry to be consistent with that space group. The only arrangement of layers compatible with this space group then, is $(AA)(\bar{A}\bar{A})(BB)(\bar{B}\bar{B})(AA)(\bar{A}\bar{A})(BB)(\bar{B}\bar{B})\ldots$.

The space group Cc symmetry is satisfied by the arrangement in which $X = \bar{C}$ and the layers are bent as $(AA)(\bar{C}\bar{C})(BB)(\bar{C}\bar{C})(AA)(\bar{C}\bar{C})(BB)(\bar{C}\bar{C})\ldots$. This configuration separates the structure into columns of anions parallel to $\underline{z}$ and bent in the C mode at $(0.3,0)$ and $(0.8,\frac{1}{2})$ in the (x,y) plane and bent in the A and B modes alternately at $(0.8,0)$ and $0.2,\frac{1}{2})$.

The arrangement produced when $X = \bar{A}$ or $\bar{B}$ is also consistent with this space group, but in the idealized model, the extra symmetry associated with the C2/c space group is also generated. The limitations of the model are such that it is impossible to rule out other shifts of atom positions in the structure which would remove these new symmetry elements and reduce this bending arrangement to Cc symmetry.

Above 520°C the crystal adopts a new symmetry consistent with the orthorhombic space group $C222_1$. Since the C centering persists, the two unique choices for the orientation of bending within a layer are (AA) or (CC). However, for the same choice of origin as in the previous cases, the space group requires that a 2_1 axis lie parallel to $\underline{a}$ at $\underline{b} = \frac{1}{4}$. Under this symmetry operation a bend A at molecule "1" produces a bend B at molecule "2" and the centering operation is lost. Therefore, only the (CC) mode of bending is consistent

with this space group.

In the idealized model, the bending in successive layers will be (CC)($\bar{C}\bar{C}$)(CC)($\bar{C}\bar{C}$)... with translationally equivalent layers separated by 13.5 Å along $\underline{z}$. This result is supported by photographs of the h0ℓ layer which indicate that the separation between unit cells is 13.5 Å along $\underline{c}$. A very few faint reflections appear at $\frac{1}{3}$ the separation along $\underline{c}^*$ indicating a tripling of the $\underline{c}$ axis length. The upper layers of the reciprocal lattice (h1ℓ, h2ℓ, etc.) show many relatively intense reflections situated at positions corresponding to $\frac{1}{3}$ the separation of strong reflections in the zeroth layer photograph. These indicate that the translational symmetry does not hold for $\underline{c}$ = 13.5 Å but the repeat distance is actually 40.5 Å along the $\underline{z}$ direction.

The tripling of the $\underline{c}$ axis cannot be accounted for by simple bending of the pyro anion in this model, but must arise from displacement of atoms in the cell, in such positions that their projection on the h0ℓ plane is unchanged. The equation

$$F_{hk\ell} = \sum_{j=1}^{N} f_i \exp 2\pi i(hx_j + ky_j + \ell z_j)$$

is an expression of equation 2.14 and shows the dependance of the structure factor on the term (hx + ky + ℓz). When k = 0, the y coordinates of atoms in the unit cell have no effect on the structure factor. The h0ℓ photograph shows that the

x and z coordinates of the atoms in the structure exhibit translational symmetry every 13.5 Å along c. When $k \neq 0$, the structure factor is no longer insensitive to the y coordinates of the atoms and the structure shows translational symmetry only every 40.5 Å along c. Therefore, the tripling of the c axis length must be a result of changes in only the y coordinates of some atoms in the structure.

A comparison of photographs from the h0ℓ plane of the room temperature phase ($P2_12_12_1$) and the same plane of the 500° phase ($C222_1$) is informative. In the latter case all h = 2n+1 reflections are missing and several large intensity changes have occurred, but the pattern of relative intensities of reflections close to each other have for the most part, remained unchanged. Thus, this projection of the structure still retains many of the main structural features of the room temperature phase.

Very little can be said with confidence concerning the bending of the anion above 600°C. The symmetry is indicative of the space group $P6_322$ and the cell dimensions have returned to those of the room temperature phase. The hexagonal unit cell dimensions are a = 5.4 Å ($9.4 \times 1/\sqrt{3}$) b = 5.4 Å and c = 13.5 Å. The anions lie on three-fold axes parallel to c at $(\frac{1}{3},\frac{2}{3})$ and $(\frac{2}{3},\frac{1}{3})$ and the chain of Na^+ ions is colinear with the 6_3 axis. If these symmetry elements are imposed on the idealized model, a linear pyro group is required with no bending allowed at the bridging oxygen atom. The Na(1) ion is

situated in the unsatisfactory 9-coordinate site, coplanar with the bridging oxygens, but fixed on the 6_3 axis. The only model that appears to satisfy the symmetry is one in which a randomized bending occurs within each layer, such that each bridging oxygen is bonded to a sodium ion, but coherence within the layer is lost and the bending averages out over the crystal to give apparent three-fold symmetry to each "average" pyrophosphate anion.

It is in this phase, however, that the assumption of a relatively rigid structure with only oxygen atoms allowed to deviate from the idealized model, is perhaps least justified and other major structural changes may have occurred in the crystal.

Conclusion

The orientation of the pyrophosphate anion in the anhydrous $Na_4P_2O_7$ crystal differs significantly from that of the anion in the decahydrate crystal structure. The P-O-P bridging angle has reduced to 127.6(2)° from 130.2° in the decahydrate. The two P-O (bridge) bonds are 1.640(2)Å and 1.632(2)Å compared to 1.612(5)Å and the P-O (outer) bond is 1.515(2) Å compared to 1.523(4)Å in the hydrate. In the anhydrous compound the sets of terminal oxygen atoms on each anion are nearly eclipsed, lying some 32° out of phase in the (x,y) projection while the decahydrate structure consists of a nearly staggered anion with one PO_4^{3-} tetrahedron out of phase by about 54° with respect to the other.

In his discussion of π-bonding in pyrophosphate and related anions, Cruickshank (4) has predicted shortening of the P-O (bridge) bond with straightening of the P-O-P bending angle. This effect should proceed gradually as the bridging oxygen proceeds from a bonding orbital hybridization state of sp^3 (bond angle = 109°) through sp^2 (bond angle = 120°) to sp(bond angle = 180°). As these changes take place, more and more π bonding is possible through the bridging oxygen atom, shortening the P-O (bridge) bonds and diverting electron density from the P-O (outer) bonds causing them to lengthen. The observed changes in bond lengths as the bending angle goes from 127.6° to 130.2° seem to be fairly large for such a small change in angle, but are in the predicted direction. The presence of water molecules in the decahydrate structure appears to have had some effect on the anion, since in the anhydrous structure, the bending angle corresponds almost exactly to the predicted "valency angle" of Hirshfeld (24) as interpreted by Cruickshank (4); whereas the angle in the decahydrate structure differs by 3°.

Corbridge (17) has pointed out that similarities exist between the crystallographic data for the tetrasodium pyrophosphate decahydrate and the corresponding hypophosphate. This trend does not seem to extend to the analogous anhydrous compounds of sodium. A comparison of the powder data for $Na_4P_2O_7$ and $Na_4P_2O_6$ listed in the ASTM files (25) shows only two

reflections that could be compared with any confidence. The 110 and 111 reflections of $Na_4P_2O_7$ lead to d-spacings of 4.67 and 4.41 respectively, and could be matched in intensity by reflections observed at 4.70 and 4.39 in $Na_4P_2O_6$. The 004 reflection at d = 3.37 in the pyrophosphate is not observed in the hypophosphate, however, and a strong (I/I_o = 0.40) reflection at d = 3.02 in the hypophosphate appears as a very weak (I/I_o = .01) reflection in the pyrophosphate at d = 3.04.

The effects of the crystal environment seem fairly large in determining similarities in structures. When the relative change in the size of formula units is considered, it seems logical to expect that although the hydrated forms of sodium pyrophosphate and hypophosphate may be structurally related, the anhydrous forms may not. The change from $Na_4P_2O_7 \cdot 10H_2O$ to $Na_4P_2O_6 \cdot 10H_2O$ removes about $\frac{1}{17}$ the volume from the formula unit; whereas the change from $Na_4P_2O_7$ to $Na_4P_2O_6$ removes $\frac{1}{7}$ the volume of the formula unit. Thus, more drastic differences in structure are to be expected in the anhydrous case.

Discussion of the structural changes that occur during phase transformations is necessarily limited by severe assumptions. The retention of the integrity of the room temperature unit cell dimensions must have significance and the doubling and tripling of the c axis during the approach to hexagonal symmetry indicates that the major changes in atomic

coordinates take place along c with small but significant activation energies between steps. The exact manner of coupling between two and even three unit cells along c during these transformations must await the elucidation of the intermediate structures.

CHAPTER V

THE CRYSTAL STRUCTURE AND PHASE TRANSFORMATIONS OF δ $Ba_2P_2O_7$

Introduction

$Ba_2P_2O_7$ crystallizes in two forms (26,27). The form stable at temperatures below 725°C (27) has been labelled α and is said to be isomorphous with the α forms of $Ca_2P_2O_7$ and $Sr_2P_2O_7$ (26). These structures although closely related are in fact different (28,29,30), with the α $Ca_2P_2O_7$ crystallizing in the monoclinic space group $P2_1/n$, a sub-group of the orthorhombic space group Pnma found for α $Sr_2P_2O_7$. Thus, although α $Ba_2P_2O_7$ is likely to be very similar to the α forms of the other alkaline earth pyrophosphates, its actual space group cannot be ascertained with the presently available data.

The high temperature form of $Ba_2P_2O_7$ is called δ and has been shown to be stable up to the melting temperature, 1430°C (27). Previously no structural research other than the x-ray diffraction pattern for the powder (26) and an infrared absorption curve (31) has been reported on the solid.

The Ca and Sr pyrophosphates in addition, show a phase stable at lower temperatures, called β, and finally a third phase γ has been reported for $Ca_2P_2O_7$. Randby et al. (26)

have investigated the luminescence of mixed alkaline earth pyrophosphates activated with Sn and Mn and from these studies a phase boundary as a function of temperature and composition has been postulated. From these curves it would appear that the β phase of $Ba_2P_2O_7$ might be stable below about 500°C. Presumably if this phase were to be stable, the sluggish nature of the phase transformation might inhibit its appearance.

Recently the known structures of the alkaline earth pyrophosphates have been compared with the alkali metal dichromates (32) and a number of the structures appearing in these systems have been correlated. These compounds generally show nearly eclipsed configurations of the anion, in the sense that when they are viewed along the Y-Y axis (Y = P, Cr) the two sets of three terminal oxygen atoms appear nearly superimposed. In addition, in each of the structures, some of the larger cations, et K^+, Sr^{2+}, bridge across the ends of the anion by sharing oxygen atoms with each of the YO_4 tetrahedra. Finally, the Y-O-Y bond angle in all of these compounds lies between 125° and 138°.

In contrast, the $X_2Y_2O_7$ compounds involving cations with radii less than about 0.9 Å show staggered anions, with the Y-O-Y bond angle ranging from 140° to 180° and with the cations bonded to only one end of a given anion.

The structure of the δ phase of $Ba_2P_2O_7$ is of some interest in considering the extent to which the discussion

of Brown and Calvo can be applied. Here as in $Cs_2Cr_2O_7$ and $Rb_2Cr_2O_7$, the size of the cation approaches or exceeds that of the oxygen atom and thus a number of structures may be possible, including some in which the cation may take up a position within a close packed array of oxygen atoms.

Experiments

Crystals of δ $Ba_2P_2O_7$ were grown by slowly cooling a melt of $Ba_2P_2O_7$ prepared from a mixture of $(NH_4)_2HPO_4$ and $BaCO_3$ in appropriate proportions to yield 35 mole % P_2O_5. The cooling program was initiated from above 1430°C, the reported melting point of $Ba_2P_2O_7$ (27), and discontinued at 1000°C. The sample was then quenched to room temperature, the rapid cooling acting to inhibit the growth of large crystals of $Ba_3(PO_4)_2$ which begin to form at 983°C in a sample of this composition. $Ba_2P_2O_7$ crystals have been prepared in this manner in about a half-dozen separate runs.

Single crystals were selected for x-ray studies with the aid of a polarizing microscope. Photographs indicated that the crystals were of hexagonal symmetry belonging to the Laue group 6/mmm, with only the ℓ=odd reflections extinct along 00ℓ. The cell dimensions were obtained and later refined to $\underline{a}$ = 9.4076(2) Å and $\underline{c}$ = 7.0749(2) Å. The density of the crystal was determined to be 4.12 gm/cc by use of a pyncometer with water as the displaced liquid. Only single crystals were used for this measurement. From these data, the number of

molecules per unit cell, Z, was found to be 3.

A feature of those x-ray photographs that included the $\underline{c}^*$ axis, was the presence of rather weak diffuse streaks lying between the layer lines and parallel to the $\underline{a}^*$ direction. Thus, δ $Ba_2P_2O_7$ at room temperature appears to be a disordered structure based upon a unit cell having a $\underline{c}$ axis equal to 2×7.07 Å, the nature of the disorder involving stacking errors of $\frac{1}{2}$ $\underline{c}$ for layers parallel to the $\underline{ab}$ plane, probably involving the bridging oxygen atom.

The nature of this disorder was investigated by cooling a crystal, mounted along the $\underline{c}$ axis, to -150°C using the apparatus described in Chapter III. At this low temperature, evidence of the diffuse streaks could not be detected. In their place, several faint reflections were observed in the $\underline{a}^*\underline{c}^*$ plane, situated between both sets of lattice rows such that the photographs of the h0ℓ and h1ℓ layers showed only spots with indicies such that h+ℓ=even, when reflections were re-indexed according to a unit cell: $\underline{a}$ = 18.8 Å and $\underline{c}$ = 14.14 Å. It is evident then that a transition to an ordered phase takes place between room temperature and -150°C. No attempt was made in this preliminary investigation to determine the exact temperature at which the transition occurs.

To investigate the structure of the room temperature phase, relative intensities of reflections in the hk0 layer were estimated from a non-integrated precession photograph by

visual comparison and a series of integrated precession photographs were taken of the h0ℓ layer. The relative intensities of reflections in this layer were measured with an optical microdensitometer. Lorentz and polarization corrections were applied to these data.

A new crystal was selected and shaped to be a rough trapezoid with both the base and the altitude measuring approximately 0.11 mm. and the top measuring 0.07 mm. It was mounted on a glass fibre and thence on a eucentric goniometer head with the wide base of the crystal flush with the glass fibre. Intensities were recorded with Zr filtered MoKα radiation using a θ-2θ scan technique on a General Electric XRD-6 Semi Automatic Diffractometer. Angular settings for each reflection were calculated and punched on cards using the computer program DIFPCH (15). The data were recorded using 5 concentric shells of sequentially larger scattering angle, assuming the lower symmetry Laue group 6/m. From 2θ = 0° to 35°, reflections in the entire hemisphere were measured to evaluate any effects of the irregular crystal shape on the intensity of scattering. Above 2θ = 35° only those reflections with positive φ values were measured; thus only one-quarter of the sphere of reflection was observed in this range. A total of 2287 reflections were measured up to a Bragg angle of 60°. This reduced to 548 unique reflections in the Laue group 6/m. However an inspection of the observed intensities led to the choice of 6/mmm as the correct Laue group. Reflections were arranged according to increasing values of sin θ/λ

and relative structure factors were averaged using unit weights for observed reflections and $1/\sigma^2$ weights for entirely unobserved reflections. The total number of unique reflections was then reduced to 332 including 86 unobserved reflections. The number of unique reflections observable using MoKα radiation was 523.

It was determined that although the limitation imposed on ϕ did reduce the number of equivalent reflections measured, a complete set of unique reflections was not contained within that limited scan range since the crystal was not mounted with a major axis parallel to the spindle axis.

Since the space group could not be uniquely determined, the Patterson function was calculated for the hk0 and h0ℓ projections using the space group with the lowest symmetry consistent with the systematic absences and six-fold symmetry. The Patterson map based on the symmetry of space group $P6_3$ revealed prominent peaks at all combinations of $\frac{1}{3}$, $\frac{2}{3}$ and 0 for both $\underline{u}$ and $\underline{v}$ directions. The h0ℓ projection showed prominent peaks at combinations of u = 0, $\frac{1}{3}$ and $\frac{2}{3}$ and w = 0, $\frac{1}{2}$. This is consistent with a barium atom at the general position $(\frac{1}{3},0,0)$ in the room temperature unit cell.

Trial Structure

A trial structure was derived from a detailed analysis of the Patterson function and refined by the method of least

squares. Fourier maps of the electron density function were calculated at various stages of refinement to aid in the analysis of the structure. Refinement was terminated when the agreement factor, R, was reduced to 25%.

The structure may be described as based on a model restricted to at least P3 symmetry. Pyrophosphate groups occur on three-fold axes at (0,0), $(\frac{1}{3},\frac{2}{3})$ and $(\frac{2}{3},\frac{1}{3})$ in the (x,y) plane of a unit cell in which $\underline{a} = \underline{b} = 9.4076$ Å and $\underline{c} = 7.0749$ Å. The bridging oxygen atoms in the three anions are coplanar at $z = 0$, and barium atoms are situated in this plane at approximately $(\frac{1}{3},0)$ and at positions related to this by the three fold axes. Another set of barium atoms exist in a plane at $z = \frac{1}{2}$ at approximately $(\frac{1}{3},\frac{1}{3})$ in the (x,y) plane and at positions related to this by the three fold symmetry. The terminal oxygen atoms of the anions are eclipsed and are in positions such that the projection of a P-O bond on the (x,y) plane is directed between the Ba positions at $(\frac{1}{3},0)$ and $(\frac{1}{3},\frac{1}{3})$. The resultant configuration consists of a Ba ion at the centre of a trigonal prism coordinated to nine oxygen atoms. Three bridging oxygen atoms are coplanar with the Ba ion at $z = 0$ at a separation of 3.1 Å. The remaining 6 oxygen atoms form two triangles at the ends of the prism and are separated from the Ba ion by $\sim$ 2.8 Å. In the sites at $z = \frac{1}{2}$, each Ba is equally coordinated to six terminal oxygen atoms with a Ba-O distance of 2.5 Å. This type of site is smaller than average but may be enlarged by distortions in

Figure 5.1

The (x,y) projection of the structure of $Ba_2P_2O_7$

Phosphorous atoms are represented by small circles and each appears superimposed on a bridging oxygen atom residing in the idealized position. Barium ions appear as cross-hatched circles. Those represented by thin lines exist at z=0 while those at z=1/2 are drawn with thick lines. Ba1 and Ba2 appear on the same level in z and merge with each other as a result of disorder in the structure. The result of disorder with regard to the anions is not shown for the sake of clarity in the diagram. Terminal oxygen atoms are eclipsed in each anion, the lower atom (OB) represented by a thin line and the upper (OA) represented by a thick line.

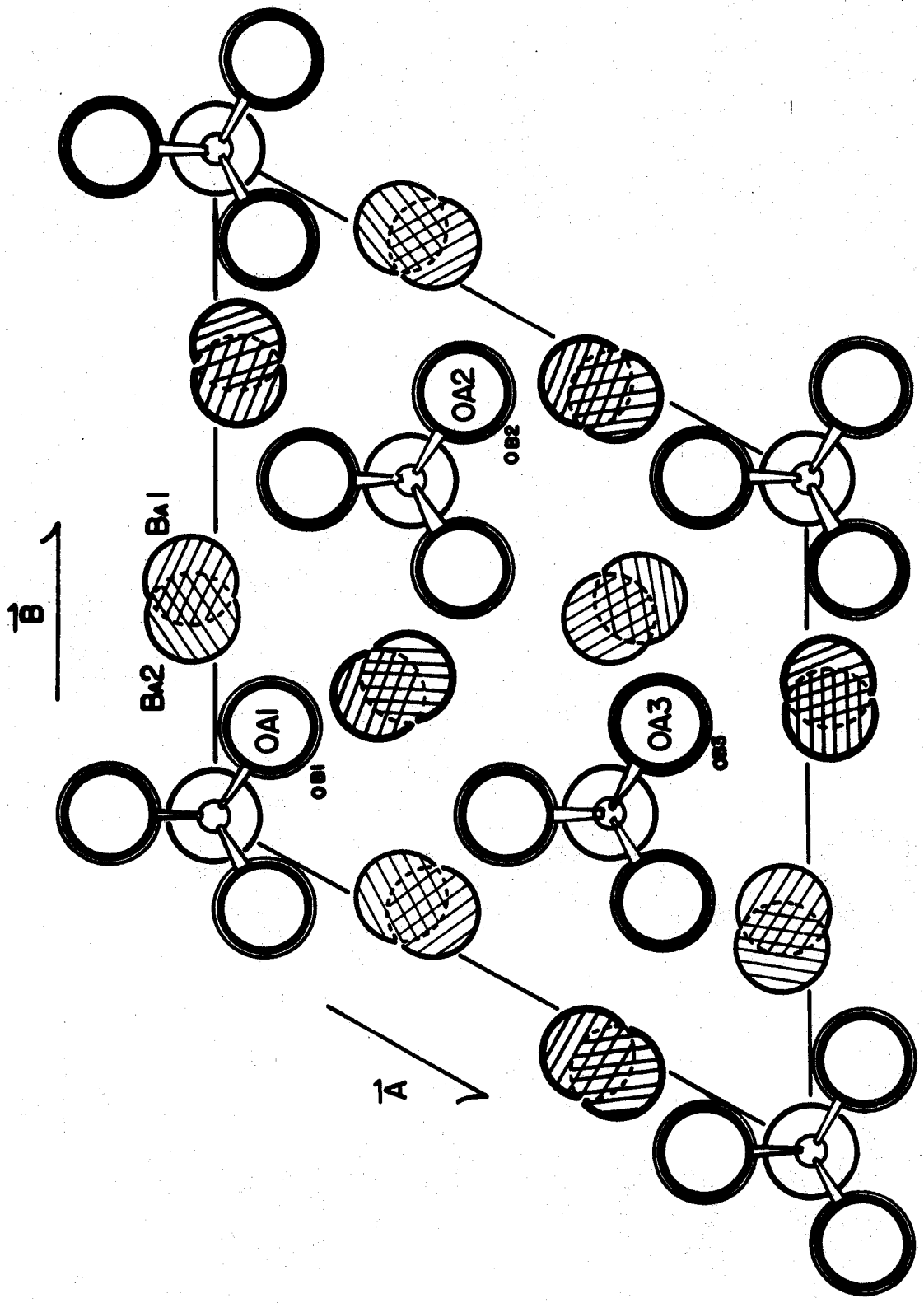
Ba1
Ba2
OA1
OA2
OA3
OB1
OB2
OB3
1B
1A

the structure which will be discussed later.

Superimposed on this basic structure is a second equivalent structure, apparently related to the first by a 6_3 symmetry operation parallel to $\underline{c}$ at (0,0) in the (x,y) plane. The barium atoms in this second structure appear to superimpose on the Ba atoms present in the first, such that in the second structure, the nine-fold coordinated Ba site is at $z = \frac{1}{2}$ and the six-fold coordinated site lies at $z = 0$. The pyrophosphate groups overlap such that terminal oxygen atoms from one structure appear nearly coplanar with phosphorous atoms from the other. Bridging oxygen atoms appear at $z = 0$ and $z = \frac{1}{2}$. This superposition cannot be interpreted as a component of the basic crystal structure, but arises in the model as a result of twinning in the crystal.

A least squares refinement of such a model with multiplicities of the atoms adjusted to provide only three molecules in the unit cell gave an unweighted R-factor of 28%.

Refinement including anisotropic temperature factors for the barium atoms showed anomalously large thermal vibration in the $\underline{a}$ direction. Electron density calculations produced from this model indicated a slight splitting in the peaks corresponding to the Ba atoms. A model with two Ba atoms moved slightly away from the $(\frac{1}{3},0)$ position was refined by least squares with the x and y coordinates of each as variables. The result was a structure in which two Ba atoms, each weighted by

$\frac{1}{2}$, exist on the same level in z and are separated by 0.5 Å rather than superimposing exactly. The unweighted "R-factor" was reduced to 25% when refinement was carried out under the symmetry restrictions of space group $P6_3$. Atomic parameters determined as a result of this refinement are presented in table 5.1 and the observed and calculated structure factors are to be found in table 5.2.

For a complete refinement of the structure to be carried out, a minimum of 55 variables must be determined. If the bridging oxygen atom shows the bending that seems typical of pyrophosphate anions (cf. 126° in $Na_4P_2O_7$), disorder about each three fold axis site is required, adding at least another 24 variables to the calculation. Since the total number of unique reflections recorded is 332, more data are required for a complete solution.

Discussion

Evidence of disorder in the crystal is observed as diffuse streaks in the room temperature x-ray diffraction pattern. The phase transition at low temperature results in loss of the apparent translational symmetry in adjacent unit cells along all three major axis directions. Presumably, unit cells that differ from the "normal" structure are distributed randomly within the crystal with a sufficient population that an average of the different structures is observed at room temperature by

TABLE 5.1 Atomic Parameter Table for δ-$Ba_2P_2O_7$

Atom	X	Y	Z	U_{iso}	U_{11}	U_{22}	U_{33}	U_{12}	U_{13}	U_{23}
Ba 1	-.042(2)*	.337(2)	0.00		.013(6)	.015(6)	.019(5)	.007(5)	0.0	0.0
Ba 2	-.044(2)	.285(2)	0.00		.007(6)	.014(6)	.021(5)	-.002(5)	0.0	0.0
OA1	.088	.176	+.287	0.02						
PA1	0.0	0.0	+.221	0.035						
CENO1	0.0	0.0	0.0	0.04						
PB1	0.0	0.0	-0.221	0.035						
OB1	.088	.176	-.287	0.02						
OA2	.421	.843	+.287	0.02						
PA2	.333	.667	+.221	0.011						
CENO2	.333	.667	0.0	0.04						
PB2	.333	.667	-.221	0.011						
OB2	.421	.843	-.287	0.02						
OA3	.755	.509	+.287	0.02						
PA3	.667	.333	+.221	0.064						
CENO3	.667	.333	0.0	0.04						
PB3	.667	.333	-0.221	0.064						
OB3	.755	.509	-0.287	0.02						

*since refinement of the structure has been limited, e.s.d.s have been listed for only those parameters that have undergone significant refinement.

TABLE 5.2

TABLE OF OBSERVED AND CALCULATED STRUCTURE FACTORS OF BARIUM PYROPHOSPHATE

UNOBSERVED REFLECTIONS ARE MARKED WITH *

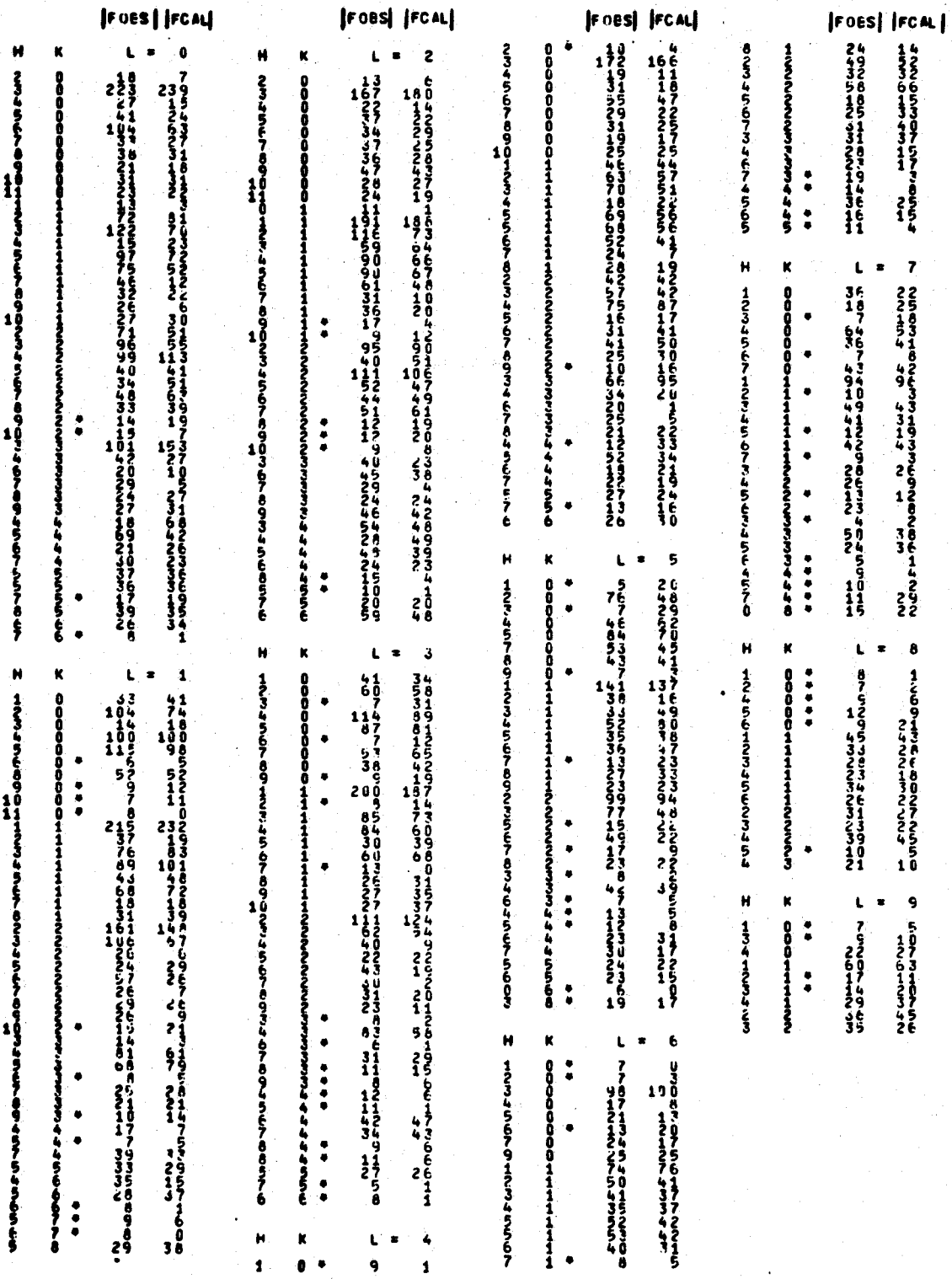

x-rays. At very low temperature, the thermal energy in the lattice is reduced sufficiently that correlation energies between neighbouring unit cells become significant and the structure is resolved into a translationally repeating unit, 8 times the volume of the unit cell at room temperature.

The occurrence of new reflections in the diffraction pattern can be understood in the following way. The expression for the structure factor

$$F_{hk\ell} = \sum_{j=1}^{N} f_j \exp(2\pi i(h\underline{a}^*x_j\underline{a}+k\underline{b}^*y_j\underline{b}+\ell\underline{c}^*z_j\underline{c}))$$

can be separated into summations from a unit cell and its neighbors. For simplicity in this example only the cell adjacent along the $\underline{c}$ direction is considered.

$$F_{hk\ell} = \frac{1}{2}\{\sum_{j=1}^{N} f_j \exp(2\pi i(hx_j+ky_j+\ell z_j)) + \sum_{j=1}^{N} f_j \exp(2\pi i(hx_j+ky_j+\ell(z_j+1)))\} .$$

This would correspond to two adjacent unit cells each with a $\underline{c}$ axis equal to 7.07 Å in length.

If a small change (δr_j) occurs in one cell, and the opposite change ($-\delta r_j$) occurs in the adjacent cell, then translational symmetry will be lost and the $\underline{c}$ axis length will double. The sums may now be expressed as extending over $\frac{1}{2}$ of the new $\underline{c}$ axis length c'

$$F_{hk\ell'} = \frac{1}{2}\{ \sum_{o}^{1/2c'} f_j \exp(2\pi i(hx_j+ky_j+\ell' z_j+\underline{H}\cdot\delta\underline{r}_j))$$

$$+ \sum_{1/2c'}^{c'} f_j \exp(2\pi i(hx_j+ky_j+\ell' z_j+\underline{H}\cdot(-\delta\underline{r}_j)))\}$$

where ℓ' represents a new set of indices referring to the new $\underline{c}$ axis. Provided $\underline{H}\cdot\delta\underline{r}_j$ is small, the factor $\exp 2\pi i\ \underline{H}\cdot\delta\underline{r}_j$ may be expressed as a power series expansion:

$$\exp(2\pi i(\underline{H}\cdot\delta\underline{r}_j)) = (1+2\pi i\ \underline{H}\cdot\delta\underline{r}_j + (2\pi i\ \underline{H}\cdot\delta\underline{r}_j)^2/2!).$$

Thus,

$$F_{hk\ell'} = \frac{1}{2}\{ \sum_{o}^{1/2c'} [f_j \exp(2\pi i(hx_j+ky_j+\ell' z_j))]\cdot[1+(2\pi i\ \underline{H}\cdot\delta\underline{r}_j)+(2\pi i\ H\cdot\delta r_j)/2!]$$

$$+ \sum_{1/2c'}^{c'} (-1)^{\ell'} [f_j \exp(2\pi i(hx_j+ky_j+\ell' z_j)]\cdot[1+(2\pi i\ \underline{H}\cdot(-\delta\underline{r}_j))$$

$$+ (2\pi i\ H\cdot(-\delta\underline{r}_j))^2/2!]$$

All reflections with ℓ' = even in the new cell correspond to reflections present for the unit cell with $\underline{c}$ = 7.07 Å . For these reflections the δr_j terms cancel in the first order and if these terms are small, they contribute only as very small "squared" terms to change the value of $F_{hk\ell'}$ from the value present for the small unit cell. This effect is observed when intensities of reflections in room temperature and low temperature photographs of the $Ba_2P_2O_7$ diffraction pattern are compared.

Reflections with indices corresponding to ℓ'=odd are present in the room temperature diffraction pattern only as

diffuse streaks. In the low temperature phase these reflections are subject to the condition $(-1)^{\ell'} = -1$ and the contributions from each half cell subtract while the $\delta\underline{r}_j$ terms add in the first order. The overall effect is to reduce the absolute value of the structure factor and thus reduce the observed intensity of each ℓ'=odd reflection. It is observed that the new spots which appear in place of diffuse streaks at low temperature are generally very weak when compared to the average ℓ'=even reflection.

Little of value has been said thus far concerning the nature of disordering in the structure. As pointed out previously, bending of the pyrophosphate anion about the bridging oxygen is fairly typical in structure of this type (28,30,19). Since each pyro group appears to be located on a threefold axis, any bending must have positional disorder associated with it. Further,the rather long bond lengths (3.1 Å) between Ba and the bridging oxygen residing on the three fold position indicate that some bending of the anion might take place to relieve this situation. However, a scheme of bending has not yet been devised that, on the average, gives the observed symmetry and unit cell size, and yet, when correlated in detail, predicts the doubling of the principal axis lengths as observed at low temperatures.

The splitting of the barium positions observed in the refinement of the structure may also be related to the bending

of the pyrophosphate groups in that one and only one bridging oxygen at z=0 will be advanced toward each Ba at z=0. The presence of this bending ensures that the environment of this Ba ion is significantly different than the cation environment at $z = \frac{1}{2}$. In the basic structure the Ba ions at $z = \frac{1}{2}$ bear no requisite crystallographic relationship to the Ba ions at z=0. Thus independent displacements are possible. Superposition of the image of the barium ions at $z = \frac{1}{2}$ on the cation positions at z = 0 (and vice versa) produces two "average" sites separated by ~ 0.5 Å on approximately the same level in z. This superposition produces Ba sites related by a 6_3 symmetry axis and thus is consistent with the apparent symmetry $6_3/mmm$. Since the Ba-Ba separation in the metal is 4.37 Å, this is the minimum separation that can be observed between cations in any realistic model of the $Ba_2P_2O_7$ structure. Thus, the superposition cannot be interpreted as a real situation in the crystal.

Another requirement of this symmetry is that an image of a pyrophosphate ion centred on z=0 be generated at $z = \frac{1}{2}$, producing apparent overlapping of anions in an impossibly crowded situation. Yet, although the Ba ions dominate the scattering, a deviation from the 6_3 symmetry axis on the part of the anion should be detectable in the x-ray diffraction pattern. Thus we are led to the conclusion that the crystal is twinned or disordered in some sense. This latter effect

could be due to a random positioning of the pyrophosphate groups such that the bridging oxygen atom lies with equal probability at either $z = 0$ or $z = \frac{1}{2}$ and should be distinguished from the temperature dependent disorder which leads to an enlarged cell at low temperature.

The intensities of reflections arising from the superposition of two differing structures in one unit cell can be understood in the following way.

If $P_{hk\ell}$ and $Q_{hk\ell}$ represent the scattering amplitude arising from each of two possible configurations in the crystal, then translational periodicity no longer strictly applies throughout the crystal and the structure factor for each reciprocal lattice point must be summed over each unit cell individually.

$$F_{hk\ell} = \sum_{n_1} \sum_{n_2} \sum_{n_3=0}^{\infty} \sum_{j=1}^{N} \exp(2\pi i(\underline{H}\cdot\underline{r}_j)+(\underline{H}\cdot\underline{L}_{n_1n_2n_3}))$$

where $\underline{L}_{n_1n_2n_3}$ is the vector from the chosen origin of the crystal to the unit cell undergoing the summation when the distribution of the configurations throughout the crystal is random, then the expression for the observed intensity of a reflection,

$$I_{hk\ell} = F_{hk\ell} \cdot F^{*}_{hk\ell}$$

includes both types of structure factors $P_{hk\ell}$ and

$Q_{hk\ell}$ and their complex conjugates. Each observed intensity is a sum of all possible combinations

$$I_{hk\ell} = P_{hk\ell}P^*_{hk\ell} + P_{hk\ell}Q^*_{hk\ell} + Q_{hk\ell}P^*_{hk\ell} + Q_{hk\ell}Q^*_{hk\ell} .$$

These parts of the sum are indistinguishable and the intensity is resolved as

$$I_{hk\ell} = (P_{hk\ell} + Q_{hk\ell})(P^*_{hk\ell} + Q^*_{hk\ell}) .$$

The expression $F_{hk\ell} = P_{hk\ell} + Q_{hk\ell}$ applies to every observed structure factor and results in an apparent superposition of the two configurations in the same unit cell when the structure is solved by ordinary methods.

It should be noted that at the present stage of refinement of the structural model, there is very little experimental evidence for the choice of an eclipsed configuration of oxygen atoms versus the staggered configuration. Only the eclipsed configuration gives results consistent with the apparent 6_3 symmetry produced by the positional disorder, but both configurations give essentially identical Ba-O separations in the idealized case and the effect on the data of the deviation from the apparent $6_3/mmm$ symmetry caused by the staggered configuration is likely to be very small. The more likely case is that the deviation of the barium ions from

the idealized positions causes distortion of the oxygen environment and the anions will assume some intermediate configuration.

Conclusion

The δ phase of $Ba_2P_2O_7$ presents a number of interesting crystallographic problems. First, although the apparent Laue symmetry is 6/mmm no reasonable structure can be found that would be consistent with this symmetry and positional disordering or perhaps crystal twinning is indicated. Another type of disorder occurs in the crystal and is distinct from the first by its dependence on temperature. This probably arises, as in other pyrophosphate systems (33) from an ordering of bent pyrophosphate ions. This latter disordering is the second interesting but unresolved problem in δ $Ba_2P_2O_7$.

δ $Ba_2P_2O_7$ clearly differs from all previously reported $M_2X_2O_7$ compounds. These are distinguished first by a nearly eclipsed versus staggered X_2O_7 configuration and second by the manner in which the oxygen atoms pack to form a three dimensional structure. In both cases the cations seem to fit into the available holes. These sites are octahedral in coordination or nearly so when the cation radius is less than that of Cd^{2+} or Ca^{2+} (∿ .99 Å) leading to thortveitite structures with the anion nearly staggered. The dichromate series generally feature cations with irregular coordinations and

some cation-oxygen bonding bridging the length of the anion.

The structure of δ $Ba_2P_2O_7$ has features more like that of $Na_4P_2O_7$ in that one cation lies at the level of the bridging atom while the other lies in an octahedral site. The structures differ however in that in $Na_4P_2O_7$ these two sites are colinear while in δ $Ba_2P_2O_7$ the large size of the Ba ion and the Ba-Ba interaction requires that they be further separated. A significant similarity in the two structures is the occurrence of phase transformations in both systems, probably based upon a bridging oxygen atom-cation interaction.

Each compound crystallizes from the melt into a form in which the anion appears to lie parallel to a three fold axis and thus, if bending occurs at the bridging oxygen, disorder is indicated with regard to the direction of that bending. In each structure, the bridging oxygen can bend toward one of three cations at the same level in z and this choice apparently gives rise to the disorder. At lower temperatures, $Na_4P_2O_7$ undergoes a series of apparently reversible phase transformations resulting in ordered phases, apparently related to differing modes of bending of the anion in various layers along z. $Ba_2P_2O_7$ also shows a transformation to an ordered phase at low temperatures. In the case of $Na_4P_2O_7$ three distinct, ordered phases are observed at temperatures below the ordering transition. It is unlikely that a corresponding

polymorphism will be observed in the barium system, since the thermal energies in the crystal lattice below liquid nitrogen temperatures are likely to be too small to overcome the required entropies of transition.

The statistics describing each system are likely to be quite similar, however, since both situations deal with one cation surrounded by an equilateral triangle of bridging oxygen atoms as a basic structure and the probability of a given distortion from that structure will be reasonably independent of the type of cation. The differences in structural details such as the cation size and the distribution of positive charge throughout the unit cell will more likely bear upon the energy required for each transition than upon the nature of physical change within the crystal.

A number of further studies are called for, before the structure of δ-$Ba_2P_2O_7$ can be fully understood. These include thermodynamic studies such as differential thermal analysis (D.T.A.), or better, specific heat (C_p) studies to establish the exact transition temperature and perhaps gain information about the entropy change involved in that transition. Electron paramagnetic resonance studies would be useful in determining the number of crystallographically independent barium sites that exist within the structure, and thus help to establish which symmetry elements are truly part of the basic structure and which arise as effects of disorder. There may be a structural similarity to $Ba_2V_2O_7$ and crystallographic

investigations of this system might prove enlightening. In any case, the phase diagram given by Randby et. al. for the alkali earth pyrophosphates (26), indicates that the δ phase also exists for mixtures of Ba and Sr pyrophosphates, leading to the possibility that such a mixed system (Sr:Ba < 7:3) might lead to phases in which the positional disorder does not occur and so help to determine the details of the basic ordered structure.

CHAPTER VI

THE CRYSTAL STRUCTURE OF $H_4P_2O_7$

Introduction

The structure of the pyrophosphate anion in various environments in the crystalline state has shown a correlation in detail between bond lengths and the configuration of the anion in the crystal field of the cations. Recently, Brown and Gibbs (35) have correlated such an effect in the silicate system with the electronegativity of the cation. The justification for such an analysis is entirely empirical and will remain so unless some progress can be made towards an understanding of the bonding characteristics of such systems on a theoretical level.

The major difficulty encountered in any realistic approach to this subject involves the large number of electrons that must be treated in order to provide a reasonable approximation to a crystal environment. In terms of this aspect of the problem, the structure of $H_4P_2O_7$ would present the best obtainable approximation to a truncated basis set; since, to a first-order approximation, the crystal can be regarded as molecular.

Some theoretical research has recently been completed by D. B. Boyd (7) in which electron density distributions have

been calculated for the $H_4P_2O_7$ system. The interpretation of these calculations is limited by lack of valid experimental correlation, particularly for the geometry and bond lengths to be expected in the anion. The determination of the structure in the crystalline state would aid interpretation of these effects. In particular, knowledge of the covalent effects of hydrogen in this case would be valuable.

Typically, the covalent effects of the hydrogen atom are very large and can greatly influence the atom to which it is bonded. The bonding of a hydrogen atom to an oxygen atom has a significant effect on other bonds to that oxygen atom. In the structure of $Se_4(HS_2O_7)_2$ the mean non-bridging S-O bond length is 1.46 Å while the S-O (-H) bond is 1.54 Å. (36) Similarly, in $RbHSO_4$, the non-hydrogen bonded S-O distances average 1.44 Å compared to 1.56 (2) Å for the S-O (-H) bond (37). In the phosphate systems, the effect of the hydrogen atom is to increase the bond lengths by 0.075 (4) Å in $Na_2H_2P_2O_7 \cdot 6H_2O$ (18) and 0.049 (5) Å in H_3PO_4 (38).

In addition, the effect of cation radius on the geometry of the crystal environment can be very large (32). $H_4P_2O_7$ represents the closest possible approximation to the form of the pyrophosphate anion in the crystalline state when uninfluenced by the radius effects of the cation.

With these factors in mind, an investigation of the crystal structure of pyrophosphoric acid was initiated.

Pyrophosphoric acid has been reported to crystallize in two forms (39), (40), neither of which has been well characterized crystallographically. Shen et al. have reported that Form I is a metastable solid crystallizing spontaneously from 79.76% P_2O_5 and has a melting point of 54.4°C. Form II is a more stable crystal form, melting at 71.5°C. They also note a sluggish phase transition from Form I to Form II at about 50°C and 1-2 atmospheres pressure.

X-ray powder data of Form II were taken by Shen et al., and found to be suggestive of an orthorhombic lattice with approximate cell parameters:

$$\underline{a} = 11.05\ (5)\ \text{Å}$$
$$\underline{b} = 19.21\ (5)\ \text{Å}$$
$$\underline{c} = 10.40\ (5)\ \text{Å}$$

However, a space group could not be assigned. These dimensions should be considered as only approximate, since a similar analysis of the ASTM powder data for Form I correctly reported the orthorhombic lattice type, but cell parameters differed by as much as 4 Å from the single crystal analysis reported below.

Crystals of both phases are extremely hygroscopic and absorb enough water from the air at normal humidity to dissolve in a matter of seconds. Once in the liquid phase, the chemical decomposes into a mixture of ortho, pyro, and higher polyphosphoric acids, approaching an equilibrium distribution with a half-life of approximately one minute (39). Thus

crystallization must always be accompanied by a recombination of chemical species to form $H_4P_2O_7$ which can then deposit on the crystal surface. Without seed crystals initiation periods can be of the order of weeks.

Experimental

Crystals of pyrophosphoric acid were prepared by exposing P_2O_5 to moist air until the appropriate amount of water was taken on by the delequescent powder. The resulting mixture was then sealed in a Pyrex bottle and heated to dissolve the remaining solid. The solution was allowed to cool and remain undisturbed for a period of two weeks. Small crystals grew very slowly and eventually formed a cake in the bottle. No crystals were found that were suitable for X-ray diffraction studies.

Crystals of pyrophosphoric acid in forms I and II were obtained through the courtesy of C. Y. Shen (Monsanto Co., St. Louis, Mo.). These crystals were of a quality not well suited to X-ray analysis, but selection of single crystals was attempted. Due to the hygroscopic nature of the compound, this had to be carried out under an atmosphere of dry nitrogen inside a glove-box. The method of selection consisted of separation of a sample of crystals on a petri dish and dropping selected ones into glass capillaries that had been predried for at least 6 hours at 400°C. The capillaries were then removed from the glove-box and immediately sealed in a

flame. To insure a complete seal, the ends of the tube were then coated in sealing wax. Selection of good quality crystals by this technique was limited by the lack of a microscope or other visual aid facility in the dry-box, and by the consistency of the crystals themselves, in that they tended to form lumps of several crystals rather than to separate as individuals.

FORM II

All samples of Form II crystals that were selected showed X-ray diffraction patterns characteristic of finely divided powder and it was concluded that the entire sample was of that consistency. Consequently, no single crystal diffraction studies of this phase could be undertaken.

FORM I:

Photographs of single crystals were taken on a Weissenberg camera with CuKα radiation. The crystal symmetry was determined to be orthorhombic with systematic extinctions such that the following conditions were observed:

h k ℓ	no conditions
h k 0	h = 2n
h 0 ℓ	ℓ = 2n
0 k ℓ	k = 2n .

These conditions lead uniquely to the space group Pbca. Axis lengths were measured from the Weissenberg photographs and assigned as:

$$\underline{a} = 17.91\ (5)\ \text{Å}$$
$$\underline{b} = 6.84\ (5)\ \text{Å}$$
$$\underline{c} = 9.48\ (5)\ \text{Å}\ .$$

No calibration for film shrinkage was attempted; thus the quoted e.s.d. values are approximate.

Two photographs (h0ℓ and h1ℓ layers) were of sufficient quality to measure reflection intensities by visual comparison. These data were corrected for Lorentz and polarization effects and the (u,w) projection of the Patterson function was calculated using 106 reflections.

Intensity data was limited to these two photographs because of the slow decomposition of the crystal into liquid, presumably due to the extremely hygroscopic nature of the compound. In the earlier stages of decomposition, the small amount of liquid around the crystal served as a lubricant on the walls of the glass capillary and the rotational motion of the Weissenberg camera resulted in continual problems of misalignment.

The density of a 79.9% P_2O_5 solution is very close to 2.0 gm./cc. (39). From observations of crystal flotation in the mother liquor, the crystal density was estimated to be

close to, but less than 2.0 gm./cc. Using the formula weight and the unit cell volume, it was calculated that the unit cell contained 8 formula units. The phaseless structure factors are listed in Table 6.1 and the crystal data is summarized in Table 6.2.

Trial Structures

A survey by Corbridge (17) of crystal data from hydrated pyrophosphates and hydrated hypophosphates of certain alkali metals indicated certain tendencies to isomorphism in their crystal structure, particularly in the case of $Na_2H_2P_2O_7 \cdot 6H_2O$ and $Na_2H_2P_2O_6 \cdot 6H_2O$. This correlation may extend, at least in part, to the acids $H_4P_2O_7$ and $H_4P_2O_6$. Mootz and Altenburg (41) have reported the crystal structure of $(H_3O^+)_2H_2P_2O_6$ and assign axis lengths in an orthorhombic unit cell of:

$$\underline{a} = 6.557\ (1)\ \text{Å}$$
$$\underline{b} = 11.634\ (2)\ \text{Å}$$
$$\underline{c} = 9.464\ (9)\ \text{Å}\ .$$

The unit cell contains four formula units and conforms to the symmetry of space group Pccn.

The $\underline{a}$ and $\underline{c}$ axes of this unit cell correspond very closely in length to the $\underline{b}$ and $\underline{c}$ axes respectively, of the pyrophosphoric acid unit cell. If the long axis were doubled to accommodate the 8 formula units found in the $H_4P_2O_7$ unit cell,

TABLE 6.1

TABLE OF OESERVED REFLECTIONS OF PYROPHOSPHORIC ACID, FORM 1

UNOBSERVED REFLECTIONS ARE MARKED WITH *

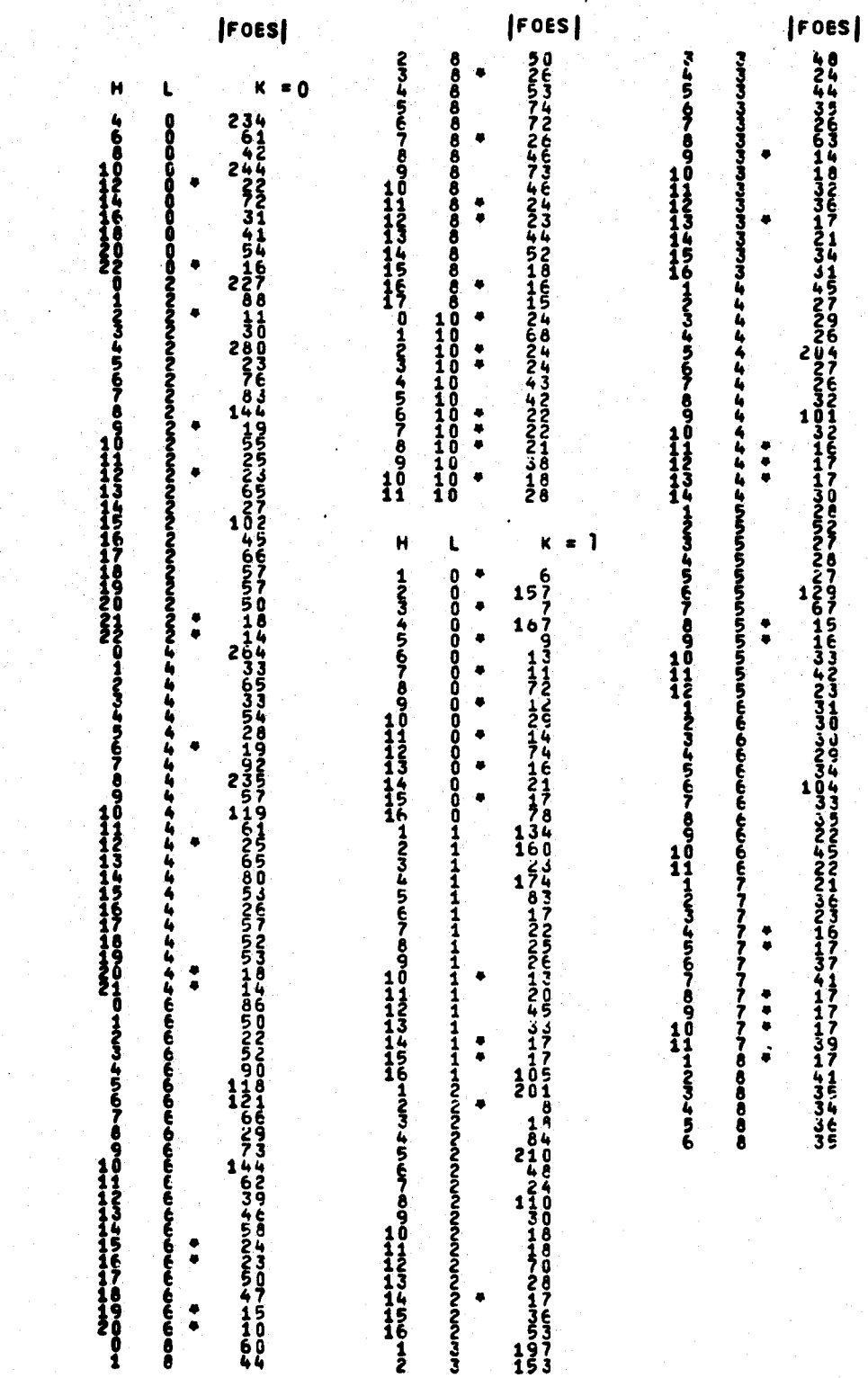

the hypophosphate structure would exhibit a 23.2 Å axis compared to 17.9 Å in the pyrophosphate. This difference appears reasonable when the position of the H_3O^+ ion is considered. Each H_3O^+ ion occurs between two $H_2P_2O_6^{2-}$ anions thus increasing the minimum distance between anions. The direction of the increase is mainly in the direction of the long axis and may explain the observed difference in this dimension. Thus,some similarities may exist between the two structures, particularly with respect to the orientation of the intramolecular P-P vector which lies parallel to the 6.8 Å axis in the hypophosphate.

However, major differences must be expected. The addition of a bridging oxygen atom between the phosphorous has the effect of lengthening the P-P separation from 2.178 Å (41) to about 3.1 Å, thus increasing the overall length of the anion to about 6.9 Å. This should be expected to impose different restrictions on the packing of oxygen atoms than exist for the P_2O_6 group and the orientation of the anion may be affected significantly. Thus traditional methods were tried in an attempt to determine the structure of $H_4P_2O_7$.

A Patterson function was calculated with the intensity data from the h0ℓ layer. The magnitudes of interactions produced by the various types of vectors expected in the Patterson function were calculated relative to the peak at the origin

TABLE 6.2

CRYSTAL DATA	
Unit cell dimensions	$\underline{a}$ = 17.91 (5) Å $\underline{b}$ = 6.84 (5) Å $\underline{c}$ = 9.48 (5) Å
Space group	Pbca
Density	D_{obs} = 2.0 gm/cc D_{calc} = 2.03 gm/cc
Molecules per unit cell	z = 8
Interatomic vectors expected in Patterson function (% of origin peak)	P-P = 3.1% P-O = 1.6% O-O = 0.9%

and are listed in Table 6.2. It was anticipated that the similarity of these relative peak heights would cause considerable difficulty in the analysis of the Patterson function. For a peak to be observed above the "background" arising from series termination and other errors, it must be the resultant of many superimposed vectors. Thus, the "heavy-atom" vectors could easily be confused with those representing phosphorous-oxygen interactions.

Since the assymetric unit is $\frac{1}{8}$ of the unit cell, the determination of the atomic coordinates for one anion will fix the corresponding coordinates of the other seven anions, unless the molecule itself contains a centre of symmetry. By inspection of the Patterson function, some of the many possible structures can be eliminated and evidence can be found to lend support to a few models of the structure.

The occurrence of major peaks in the Patterson function (figure 6.1) projected down the v axis at ω=0 and, by symmetry, at $\omega = \frac{1}{2}$, is an indication that at least the phosphorous atoms are located near the plane at z = 0 or z = $\frac{1}{4}$. The second strongest set of peaks are located at $\omega = \frac{1}{4}$. Since this represents a distance of approximately 2.36 Å in z, and the perpendicular distance between layers of close packed oxygen atoms is typically 2.42 Å, the feature may be indicative of a nearly close packed array of oxygen. Given such an array, the effective volume of the unit cell should be

Figure 6.1

The (u,w) projection of the Patterson function of $H_4P_2O_7$. Maxima are represented by the symbol +, or in the case of an elongated peak, the symbol +—+ . Contour lines are drawn in increments of $\frac{1}{16}$ P_{oo} at levels from $\frac{1}{16}$ to $\frac{1}{4}$ of the origin peak. For levels higher than $\frac{1}{4}$ P_{oo}, the increment is increased to $\frac{1}{8}$, for purposes of clarity in the diagram. The asymmetric zone is represented by $\frac{1}{4}$ of the unit cell.

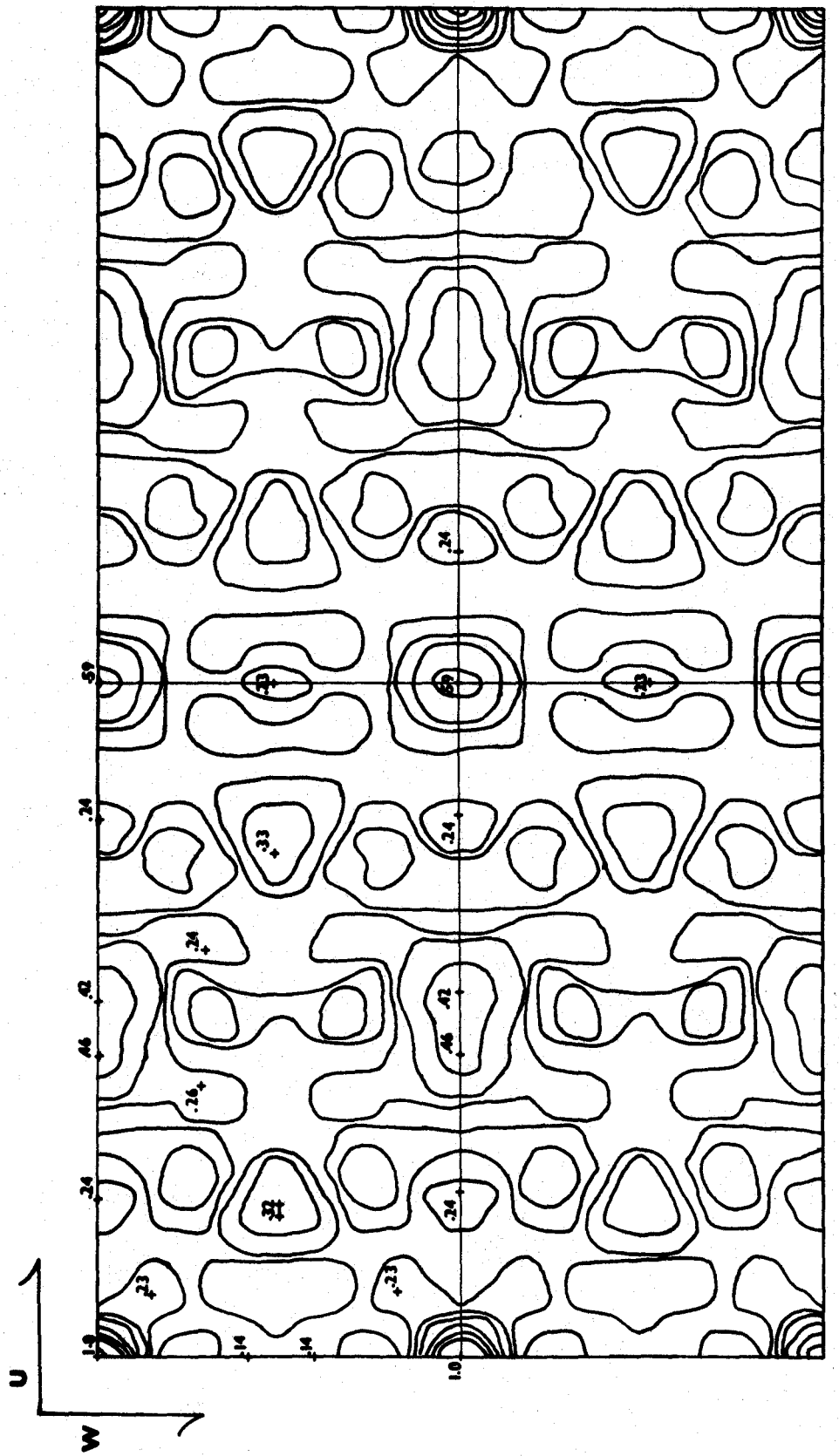
U
W
2Å

about 19 $\mathring{A}^3$ × 56 (the number of oxygen atoms in the unit cell). In this case, the effective volume per oxygen atom is about 20.8 $\mathring{A}^3$; thus, rigorous close packing cannot be assumed, but some restrictions on oxygen positions may be determined.

One direction in which packing restrictions may apply is parallel to c, since this axis length very nearly coincides with 4 × 2.4 Å, the typical interlayer separation of close packed oxygen atoms. If the packing occured along a plane defined by two principal axes, then either a or b must be a multiple of 2.8 Å, the effective diameter of an oxygen atom. Neither axis meets this requirement. Either the packing is not rigorously close, perpendicular to c or it occurs along some other plane in the cell possibly defined by c and a vector in the ab plane.

These characteristics, together with the expected P-P distance in the anion of about 3.1 Å were used as clues in interpretation of the Patterson function. A significant feature of the function is the appearance of an approximate mirror plane at u = $\frac{1}{4}$ indicating either a "pseudo-glide plane" or the projection of a pseudo-mirror plane interleaved between the a glide planes such as to be separated from them by this value. Either of these pseudo-symmetry operations leads to a peak at (0.5,0) whose magnitude relative to the peak at the origin indicates the fraction of the total electron density in

the structure that satisfies this symmetry. Further, the lack of a peak at this position in the generalized Patterson function would indicate that this pseudo-operation is restricted to the u and w coordinates alone, or at best is a mixture of a mirror and a glide plane.

If one assumes that the phosphorous atoms are related by the pseudo symmetry, two models result. One consists of the 16 phosphorous atoms distributed near two planes separated by $\frac{1}{2}$ $\underline{c}$ with the individual phosphorous atoms in the plane separated by approximately $\frac{1}{8}$ $\underline{a}$. This possibility appears unlikely since each phosphorous has neighbors at n × $\underline{a}/8$ with n = integer and thus one expects peaks at n × $\underline{u}/8$ with amplitude $\frac{450}{874}$ or .49 P_{oo} where P_{oo} is the origin peak of the Patterson function. Since the peaks found are not this large, this model can be rejected.

The second model consists of phosphorous atoms near planes separated by $\frac{1}{4}$ $\underline{c}$ with individual phosphorous atoms having z coordinates in groups of four at n $\underline{c}/4$ with n = 0,1,2,3. Such an interpretation suggests that the peak at (.25,.50) corresponds to the P-P interaction within the anion. Since this separation is slightly in excess of 3.1 Å, the v separation for these phosphorous atoms must be zero and a positive peak should be present in the generalized Patterson function at this point. Unfortunately the peak is negative, but of such a magnitude (.12 P_{oo}) as to not exclude this model. Large

positive peaks are also predicted by this model at (0.5,0) and (0.5,0.5) in the generalized Patterson function. In the latter case a negative peak with intensity in excess of -.25 P_{oo} is found. Thus this model does not appear promising although a suitable distribution of anions which can support a three dimensional scheme of hydrogen bonding can be found.

If this trial structure is to be set aside, only two basic models remain to be discussed. The first consists of the pyrophosphate anion lying parallel to b, giving two superimposed phosphorous atoms in each anion when projected on the (x,z) plane. This model is supported by the fact that the length of b (6.84 Å) is very similar to the length expected for a P_2O_7 anion with typical P-O bond lengths and geometry (6.9 Å). It is noted that within a radius of 1.5 Å from the origin, evidence of eight-fold P-O interactions is expected. All of the area within this radius is above the required intensity of .12 × P_{oo}. The model consists of sets of 4 molecules separated by $\frac{1}{2}$ in z and each member separated by approximately $\frac{1}{4}$ in x. Each phosphorous pair is surrounded, in projection, by four similar pairs ∿ 4.6 Å away. When the expected P-O bond distances are taken into account, a suitable scheme of hydrogen bonding can be devised between terminal oxygens of anions on the same level in y. However, certain peaks observed in the Patterson function are very difficult to account for with this model. In particular, the separation

of $\frac{1}{c}$ between anions, as predicted by the model, requires that only O-O vectors can contribute to peaks observed at $w = \frac{1}{4}$ and u = .10, .38 and .50. To satisfy the observed intensities of $\sim .32 \times P_{ooo}$, the interaction corresponding to the first peak must represent the superposition of 32 O-O vectors. This seems unlikely for most reasonable configurations of the anion.

The second remaining model is very similar to the first, with the exception that the P-P vector within the anion is inclined by 18° to the $\underline{b}$ axis. This is equivalent to assigning the intramolecular P_1-P_2 interaction to the peak at (.04, .08). The peak at (.10,.25) may now be considered as arising from the interaction of two centrosymmetrically related phosphorous atoms with contributions possible from P-O vectors. The P_1-P_2 separation in the y direction should be very close to $\frac{1}{2}\ \underline{b}$ and thus a negative contribution to the generalized Patterson function is expected. The terminal oxygen atoms of each anion are separated by about $\frac{3}{4}\ \underline{b}$ and should make very little positive contribution to the generalized Patterson, indicating that an overall negative peak should be expected at (.04,.08). The area is in fact positive but the possibility that a small negative peak is masked by the edging of the origin peak at this point cannot be eliminated.

The strong peaks at (.22,0) and (.28,0) can be interpreted as vectors between symmetry related phosphorous

atoms and may be considered as Harker peaks. By examination of the equivalent positions of the space group it can be shown that these peaks arise from interactions between positions such as x,y,z and $\bar{x},\bar{y},\bar{z}$. By subtraction:

$$x - (-x) = .22 \qquad z - (-z) = 0$$
$$x = .11 \qquad z = 0$$

or

$$x - (-x) = .28 \qquad z - (-z) = \frac{1}{2}$$
$$x = .14 \qquad z = \frac{1}{4} .$$

Since the condition can only be met when $z = 0$ or $\frac{1}{4}$, four possible positions are indicated for one phosphorous atom:

$$(.14,0)$$
$$(.14,\tfrac{1}{4})$$
$$(.11,0)$$
$$(.11,\tfrac{1}{4}) .$$

Using these possible positions, preliminary least squares refinements were carried out on the various models described above, including two phosphorous atoms per molecule only. The agreement factors produced with the $h0\ell$ projection data were all similar ($R \sim .50$). Electron density maps were calculated for the projection in each case but attempts to locate the positions of oxygen atoms and so refine the structure proved unsuccessful.

TABLE 6.3

Powder diffraction pattern of $H_4P_2O_7$ Form II

(Lines are indexed according to the orthorhombic unit cell dimensions $\underline{a}$ = 17.15 Å , $\underline{b}$ = 6.67 Å, $\underline{c}$ = 9.64 Å

d_{obs} (Å)	d_{calc} Å	hkℓ	I/I_o(obs)
5.49	5.495	011	21
5.33	5.265	210	25
4.82	4.82	002	90
4.77			30
4.67	4.64	102	90
4.54	4.62	211	2
4.25	4.29	400	5
4.16	4.20	202	5
3.86	3.91	012	60
3.79	3.80	112	20
3.52	3.55	212	50
3.30	3.33	020	70
3.23	3.23	501,312	100
3.18	3.20	402	15
3.04	3.05	510	10
2.98	3.00	203	5
2.76	2.76	321	30
2.67	2.71	122	15
2.63	2.63	420,610	20

Conclusions

It is concluded that more data of better accuracy is needed to successfully resolve the structure. Data involving the (y,z) projection would be very valuable, confirming the orientation of the P_1-P_2 vector in the anion and in determining the angle of bending about the bridging oxygen atom. Some packing restrictions will no doubt apply to the oxygen atoms, particularly along the 9.4 Å direction, but it is essential to know the bending angle in the anion before a definite evaluation of these restrictions can be made.

Since the phase transition between Form I and Form II seems to be a slow, gradual one, the molecular configurations are probably very similar in both phases.

It is reasonable then, to assume that the unit cell dimensions found for Form II by Shen et al. (40) are approximately correct and that the transition involves a change in anion geometry along the b direction, doubling the b axis and resulting in new unit cell dimensions

$$a = 17.91 \text{ Å}$$
$$b = 13.68 \text{ Å}$$
$$c = 9.48 \text{ Å}.$$

The orthorhombic symmetry should be retained. However, comparison of the expected "d-spacings" from such a cell and the observed d-spacings for Form II reveals significant discrepancies. Nevertheless it seems clear that a gradual phase transi-

tion does take place. Strong lines in the powder pattern of Form I can, for the most part, be found with relatively similar d-spacings in the observed pattern of Form II. If the indices of strong lines in the former are assigned to the nearest strong line in Form II, the 002, 211 and 402 reflections can be assigned d-spacings. These indicate unit cell dimensions of:

$$\underline{a} = 17.15 \text{ Å}$$
$$\underline{b} = 6.67 \text{ Å}$$
$$\underline{c} = 9.64 \text{ Å}.$$

Thus a primitive fit to the observed d-spacings can be achieved with changes in the unit cell of less than an angstrom in any given axis (cf. Table 6.3). If this is indeed the case, the phase transition probably involves a shift in the hydrogen bonding configuration in the crystal, but no major changes in the anion geometry and orientation.

CHAPTER VII

GENERAL CONCLUSIONS

Anhydrous sodium pyrophosphate has been shown to undergo three reversible phase transformations at high temperature during which the room temperature unit cell dimensions remain nearly an integral fraction of each structure. The different phases appear to be related to different modes of mutual bending about the bridging oxygen atom, available to the anions. In the room temperature phase, the symmetry prevents any displacement from producing a resultant dipole moment in the crystal but the monoclinic phase observed above 400°C is not subject to the same restrictions and it is possible that this phase may exhibit some form of ferroelectricity.

The δ phase of $Ba_2P_2O_7$ is metastable at room temperature and does not appear to be related to the α phases of $Sr_2P_2O_7$ or $Ca_2P_2O_7$. The crystal structure is disordered at 25°C but assumes a previously unreported, ordered structure at low temperatures (-150°C). This temperature dependent disorder is closely related to the situation in the highest temperature phase of $Na_4P_2O_7$ and the statistics describing the bending of the anion are likely to be similar in both

cases. The positional disorder observed at room temperature may be the result of twinning in the crystal and if so will be strictly independent of temperature. Careful study may be necessary to resolve the basic structure. The extra symmetry produced by the positional disorder has prevented the resolution of whether the conformation adopted by the terminal oxygen atoms in each anion is eclipsed or staggered. Thus the effect of cation size on the structure cannot be evaluated at this stage.

The structure of $H_4P_2O_7$ will remain unresolved until a more complete data set can be obtained. The lack of a scale factor between the zero and first layer data is unfortunate since it places very serious restrictions on the reliability of analysing the (u,w) projection of the Patterson function in terms of the generalised Patterson produced from the first layer data. Nevertheless, the unit cell dimensions and the symmetry of the structure have been determined and the possible structure has been reduced to one of three related models.

BIBLIOGRAPHY

1. Felsche, J., J. Less Common Metals, 21 (1970) 1-14.

2. Baglio, J. A., Dann, J.N., Technical Report 70-134.2, General Telephone and Electronics Lab., Bayside, New York, 11360.

3. Partridge, E. P., Hicks, V., Smith, G.W., J. Am. Chem. Soc. 63 (1941) 454.

4. Cruickshank, D.W.J., J. Chem. Soc. (1961) p. 5486.

5. Baur, W. H., Trans. Am. Cryst. Assn., 6 (1970) 129.

6. Beagley, B., Trans. Faraday Soc. 61 (1965) pt. 9, 513.

7. Boyd, D.B., Theoret. Chem. Acta. 18 (1970).

8. Lipson, H., Cochran, W. The Determination of Crystal Structures, G. Bell and Sons, London, (1967).

9. International Tables for X-ray Crystallography, Vol. II, Kynoch Press, Birmingham (1962).

10. Cruickshank, D. W. J., Pilling, D.E., Bujosa, A., Lovell, F.M., Truter, M.R. ; Computing Methods and the Phase Problem in X-ray Crystal Analysis, Pergamon Press, New York (1961).

11. Buerger, M.J., X-ray Crystallography, John Wiley and Sons, New York (1962).

12. Alexander, L.E., Smith, G.S., Acta Cryst. 15 (1962) 983.

13. Krishnamachari, N., private communication.

14. Stephens, J.S., Ph.D. Thesis, McMaster University (1967).

15. X-ray Computing System, University of Maryland.

16. Handbook of Chemistry and Physics, (1967), 48th ed., The Chemical Rubber Co.

17. Corbridge, D.E.C., Acta Cryst. 10 (1957) 85.

18. Collin, R. L., Willis, M., Acta Cryst. 27 B (1971) 291.

19. McDonald, W.S., Cruickshank, D.W.J., Acta Cryst. 22 (1967) 43.

20. MacArthur, D. M., Beevers, C.A., Acta Cryst. 10 (1957) 428.

21. De Wolff, P., X-ray Diffraction Powder Data Files, A.S.T.M. Card No. 10-187.

22. Hauptman, H., Karle, J., Acta Cryst., 9 (1956) 635.

23. Karle, I. , Proceedings of the 1969 International Summer School on Crystallographic Computing at Ottawa, Munksgaard.

24. Hirschfeld, F. L., Israel J. Chem. 2 (1964) 87.

25. X-ray Diffraction Powder Data Files, A.S.T.M., Card No. 10-187, 11-366.

26. Randby, P. W., Mash, D. H., Henderson, S. T., Brit. J. of Appl. Phys., Supp. 4 (1955) 18.

27. McCauley, R. A., Hummel, F. A., Brit. Ceram. Soc. Trans. 67 (1968) 619.

28. Hagman, L.-O., Jansonn, I., Magnéli, C.,Acta Chem. Scand. 22 (1968) 1419.

29. Calvo, C., Leung, K.Y., Stager, C.V., J. Chem. Phys. 49 (1968) 3653.

30. Calvo, C., Inorganic Chem. 7 (1968) 1345.

31. Fonda, G.R., private communication.

32. Brown, I. D., Calvo, C., J. Solid State Chem. 1 (1970) 173.

33. Robertson, B.E., Ph.D. Thesis, McMaster University (1967).

34. International Tables for X-ray Crystallography, Vol. I, Kynoch Press, Birmingham (1962).

35. Brown, G.E., Gibbs, G.V., Am. Mineralogist 54 (1969) p.1528.

36. Crump, D., Ph.D. Thesis, McMaster University (1971).

37. Ashmore, J.P., Ph.D. Thesis, McMaster University (1971).

38. Cole, F.E., Ph.D. Thesis, Washington State University (1966).

39. Van Wazer, J.R., Kirk Othmer Encyclopedia of Chemical Technology 2nd ed. (1968) 15, pp. 232-276.

40. Lyons, J.W., Shen, C. Y., Nelson, G.D., Inorganic Chemicals Div., Monsanto Co. (private communication).

41. Mootz, V.D., Altenburg, H., Acta Cryst. 27B (1971) 1520.